 doi:10.20944/preprints202107.0066.v1

*Article*

# Mechanism of the Sleeper-Ballast Dynamic Impact in Void Zones

**Mykola Sysyn[1*], Michal Przybylowicz[1], Olga Nabochenko[2], Jianxing Liu[3]**

[1] Institute of Railway Systems and Public Transport, Technical University of Dresden; Dresden, Germany; mykola.sysyn@tu-dresden.de
[2] Dnipro National University of Railway Transport named after Academician V. Lazaryan; Dnipro, Ukraine; rsk_lf@diit.edu.ua
[3] MOE Key Laboratory of High-speed Railway Engineering, Southwest Jiaotong University; Chengdu, China; jianxingliu@my.swjtu.edu.cn

* Correspondence: e-mail@e-mail.com; Tel.: (optional; include country code; if there are multiple corresponding authors, add author initials)

**Abstract:** Unsupported sleepers or void zones in ballasted tracks are one of the most recent and frequent track failures. The void failures have the property of intensive development that, without timely maintenance measures, can cause the appearance of cost-expensive local instabilities like subgrade damages. The reason of the intensive void development lies in the mechanics of the sleeper and ballast bed interaction. The particularity of the interaction is a dynamic impact that occur due to void closure. Additionally, void zones cause inhomogeneous ballast pressure distribution between the void zone and fully supported neighbour zones. The present paper is devoted studying the mechanism of the sleeper-ballast dynamic impact in the void zone. The results of experimental in-situ measurements of rail deflections showed the significant impact accelerations in the zone even for light-weight slow vehicles. A simple 3-beam numerical model of track and rolling stock interaction has shown the similar to the experimental measurements dynamic interaction. Moreover, the model shows that the sleeper accelerations are more than 3 times higher than the corresponding wheel accelerations and the impact point appear before the wheel enters the impact point. The analysis of ballast loadings shows the specific impact behaviour in combination with the quasistatic part that is different for void and neighbour zones, which are characterised with high ballast pre-stressed conditions. The analysis of void sizes influence demonstrate that the impact loadings, wheel and sleeper maximal accelerations appear at certain void depth after which the values decrease. The ballast quasistatic loading analysis indicates more than twice increase of the ballast loading in neighbour zones for long voids and almost full quasistatic unloading for short length voids. However, the used imitation model cannot explain the nature of the dynamic impact. The mechanism of the void impact is clearly explained by the analytic solution using a simple clamped beam. A simplified analytical expression of the void impact velocity shows that it is linearly related to the wheel speed and loading. The comparison to the numerically simulated impact velocities shows a good agreement and the existence of the void depth with the maximal impact. An estimation of the long-term influences for the cases of normal sleeper loading, high ballast pre-stress and quasistatic loading in the neighbour zones and high impact inside the void are performed.

**Keywords:** ballasted track, unsupported sleepers, sleeper-ballast dynamic impact, dynamic simulation, analytic solution, discrete element modelling

## 1. Introduction

Ballasted track local instabilities are usually related to the intensive sleeper void development that requires enormous maintenance costs and influences track reliability, availability and safety. The appearing of the void zones is unavoidable in such structures as transition zones, turnouts, rail joints etc. The maintenance cost reduction using operational and structural measures would require the plausible prediction of void and result-

Preprints (www.preprints.org) | NOT PEER-REVIEWED | Posted: 2 July 2021 doi:10.20944/preprints202107.0066.v1

ing track geometry development. However, different to the track without voids, the ballast layer settlement behaviour in void zone is influenced by many factors. Ballast layer in void zone is subjected to the special dynamic interaction that includes the different frequencies and time-shifted impact oscillations, quasistatic rail loading and contact interaction. The role of the geometrical void parameters is ambiguous (Fig. 1): on the one side increase impact loading on the other side it could reduce the quasistatic component due to its redistribution to the neighbour sleepers.

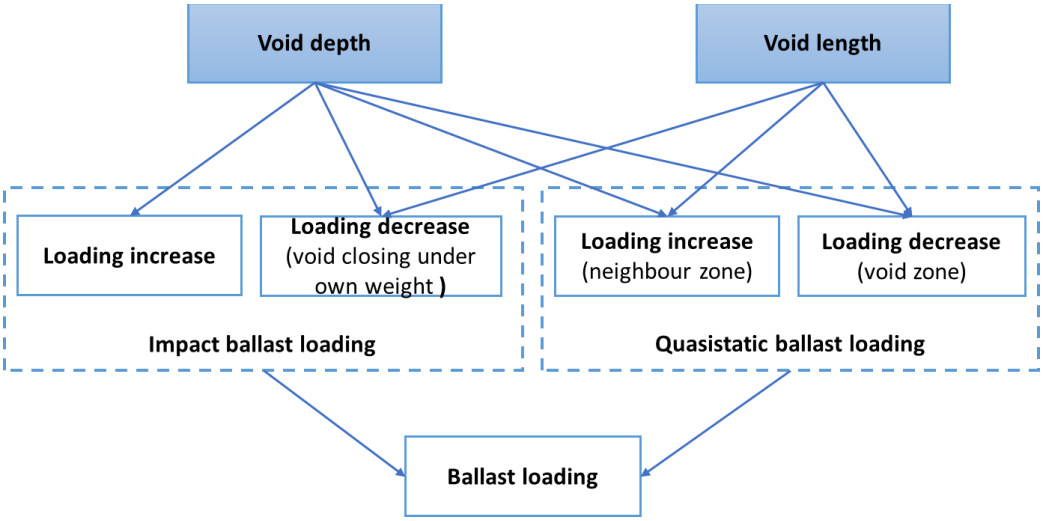


**Figure 1** Influence of the void sizes on ballast loading

The phenomenon of sleeper-ballast dynamic impact in the void zone can be schematically explained as in Fig. 2. After the wheel entering the void zone, the rail-sleeper grid is deflected so that the maximal deflection reaches the void depth. The time moment is the impact moment of the sleeper mass. After that, the void is closed and the ballast is loaded by the quasistatic wheel loading that is however, to some extent lower that for the normal track due to the loading redistribution on the neighbour sleepers.

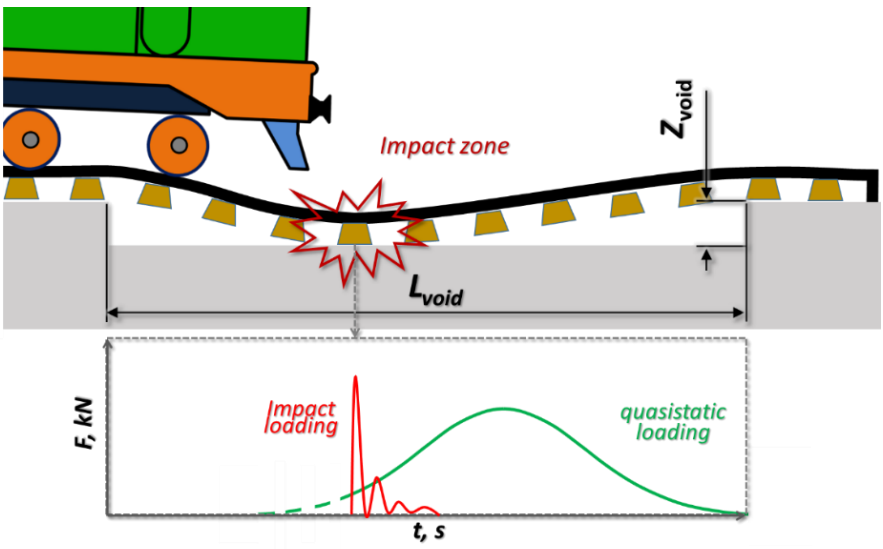


**Figure 2** Schematic explanation of the phenomenon of sleeper-ballast dynamic impact in the void zone

The values of the impact and the quasistatical loading depend on the void sizes, trail velocity and other factors. The aim of the present paper is studying the influence of the

 doi:10.20944/preprints202107.0066.v1

void sizes on the the short-time interaction behaviour in the void and neighbour zones by numerical simulation. The mechanism of the void impact is aimed to be explained by using the analytical model. Additionally, a short estimation of long-term settlement behaviour for one sleeper for the cases of normal sleeper loading, high ballast pre-stress and quasistatic loading in the neighbour zones and high impact inside the void are aimed using discrete element modelling.

## 2. Review of the literature

Until now, there were many studies to the dynamic interaction in zones with unsupported sleepers. However, the most of them are theoretical and generally without the experimental comparison and validation.

One of the earliest studies to the dynamic behavior of railway track with unsupported sleepers is presented in the paper [1]. The dynamic response of railway track with a section of unsupported sleepers is examined experimentally and using a mathematical model. An extensive study on the sleeper void short- and long-term dynamic behaviour is presented in the thesis [2]. The applied FEM simulations with the constitutive model of hypoplasticity that enables long-term dynamic settlement prediction on the development of voids between sleeper and ballast. Additionally, the influencing factors of the load level and vibrations were taken into account and the resulting phenomenological settlement equation is proposed. Another theoretical study [3] presents a FEM modelling of the sleeper contact impact due to unsupported sleepers. The modelling simulates several hanging sleepers with void depth up to 1 mm. The results indicate the increase of the sleeper-ballast contact force at the neighbouring sleepers up to 70 % for a single hanging sleeper with 1 mm void. A track system model with hanging sleepers using multi-body system (MBS) modelling and finite elements modelling (FEM) techniques is presented in the study [4]. The influence of the hanging sleepers is assumed in the calculation of the ballast-sleeper interaction as a bi-linear function. The model simulated the impact of vibrations because of hanging sleepers on the vehicle and on the track. The research [5] presents a multibody vehicle–track model assembly that couples the integration of the continuous and discrete system. The model considers an uncontacted spring-damping element underneath the unsupported sleeper as well as a triangularly unsupported sleeper. The presence of a critical gap size causing the largest force is found and is estimated to 2.5 mm for 4 unsupported sleepers. An experimental investigation and numerical simulations the dynamic behavior on unsupported sleepers is presented in [6]. A simple method for the unsupported sleepers identification using falling weight deflectometer is proposed. The numerical simulations that were based on discrete element modelling has shown different loading patterns of fully supported and unsupported sleepers. The study [7] investigates the effect of unsupported sleepers on the load of wheel/rail using a numerical simulation based on a coupling dynamic model of vehicle–track. The vehicle is modeled as a multi-body system, and the track is considered as a 3-layer model with rails, sleepers, and ballast masses. A nonlinear spring and damper are used to simulate a gap between the unsupported sleeper and the ballast mass. A detailed finite-element track model for non-periodic and asymmetrical mechanical defects were developed in [8]. The model takes into account the unsupported sleepers and the non-linear multi-body railroad vehicle system. The results are reported for different values of the forward velocities that show up to 30% increase in the wheel–rail contact forces at higher speeds. The paper [9] presents a numerical model and experimental measurements of the dynamic loads on the ballast caused by trains passing a transition zone with hanging sleepers. The results show that the forces on the ballast vary significantly both in time and space on a transition, especially with the appearance of voids under the sleepers. A parametric study comprising non-linear dynamic analyses using a FEM model of the track with sleeper voids is presented in the paper [10]. Hanging sleepers were found to be strongly associated to critical situations of track degradation.

 doi:10.20944/preprints202107.0066.v1

The performance assessment of a transition zone with unsupported sleepers by means of numerical analysis is shown in the study [11]. The stress redistribution towards the free ends of the void zones is analysed. A critical train speed is identified for the transition zone. The study [12] demonstrates the monitoring of distributed strain of rail during train passage over the bridge track with unsupported sleepers by applying a distributed optical fiber sensor. The distributed strain in the rail was measured within a length of 40.26 m and with a spatial resolution of 31.1 cm. The study could identify the location of the excessive strain due to an influence of unsupported sleepers on girder of the bridge. The research [13] investigates the response of rails due to unsupported sleepers and insulated rail joints using an elastic-plastic FEM framework. The findings showed the high sensitivity of plastic flow and rail material fatigue to the value of rail deflection.

Experimental investigation of the train induced ground vibration at a test site with under-ballast plates is presented in the paper [14]. Hammer excitations of the soil and the tracks as well as train passages indicated the presence of many voids between the sleepers and the ballast. A vehicle-track coupled dynamic model for heavy-haul freights with double suspension systems was built in [15], considering hanging sleepers. The results show that unsupported sleepers influence the aggravation of the wheel/rail interaction and affect the dynamic characteristics of the adjacent track structure with normal sleepers. The influence of the magnitude of the applied falling weight deflectometer (FWD) load on the measured track support stiffness is studied in [16]. The FWD tests were produced on full scale ballasted track models consisting of seven sleepers. It was shown that the track support stiffness measured by FWD is decreased due to the hanging sleepers. The effects of hanging sleepers and that of locally deteriorated substructure is investigated it the study [17]. Two numerical solutions were used for the simulation of track-substructure-ground response: the frequency-domain solution using a combination of beam elements for the track and FEM model. The track vibrations were simulated and compared with other studies. The effects of the gap beneath the unsupported sleeper and the track support stiffness on increasing the sleeper displacement and track support force are studied in [18] using MBS and FEM numerical simulations. A series of regression equations were derived for the peak particle velocity in the surrounding environment of railway track and the sleeper support stiffness for unsupported sleepers and fully supported ones.

An influence of the number and the distribution of unsupported sleepers in longitudinal direction on track structure is studied in [19] using numerical simulations. Dynamic responses of track structures were analyzed in cases of normal sleeper, single unsupported sleeper, two continuous unsupported sleepers and two interval unsupported sleepers. The results show that the track response of two continuous unsupported sleepers is significantly greater than that of the other two conditions. A vehicle-track coupled dynamics model that takes into account the differential ballast settlements and unsupported sleepers is presented in [20]. The research approach was based on an iterative method for acquiring the mapping relationship between the ballast settlement and the deflection of rail and sleepers. The results indicate that the superstructure settle along with the ballast bed, and sleepers are likely to become unsupported when the settlement amplitude is large or when the settlement wavelength is small. The paper [21] presents a track modeling approach based on a wave analysis technique for multi-coupled periodic structures. The approach efficiently models a track with varying characteristics in the longitudinal direction and predicts railway induced vibration due to parametric excitation. A case study is presented investigating a track with a transition zone with unsupported sleepers between ballasted and slab track.

A 1:5 scale laboratory model together with a numerical simulation model were used to study the dynamic behaviour of unsupported sleepers in the paper [22]. Both experimental and simulation results show the increase of the dynamic interaction caused by the hanging sleepers. The paper [23] demonstrates an analytical and finite-element solutions to the problem of a vibrating beam, fully or partly supported by an elastic foundation. The influence of the foundation stiffness and rail pad stiffness on the sleeper bending-mode eigenfrequencies is studied. A 3D numerical model of track was applied in the research

 doi:10.20944/preprints202107.0066.v1

[24] to study the impact of unsupported sleepers on the dynamic behavior of railway track. The model assumed the pre-stressing forces, variations of the sleeper cross-section along its length, losing or recovering contact between the sleeper and the ballast layer. An experimental model validation for case of the void-free sleeper support is shown. Studying the effects of various train bogie patterns on performance of ballasted railway tracks with unsupported sleepers is presented in the study [25] using a coupled 1D track model with MBS vehicle model. Studying the turnout dynamic phenomena of unsupported sleepers using a 3D FEM model for is demonstrated in paper [26]. Various support conditions, velocities and positions of unsupported bearers for fibre-reinforced foamed urethane bearers are studied. The results show good performance of the bearers. A 3D coupled vehicle and ballasted track interaction model development is presented in [27]. The vehicle is modeled as a multi-rigid-body system and the track-subgrade interaction is modelled by 1D finite element method. The model was applied for simulation of the soil elasticity unevenness and the contact break due to hanging sleepers. Moreover, discrete element method was introduced to model the railway ballast layer. The study [28] presents a computation scheme of the moving element method for the analysis of high-speed train-track dynamics. This numerical approach is presented as more accurate and efficient as the standard FEM in dealing with various train-track dynamic problems. The research results show that the highest maximum rail-wheel contact force is observed to occur when the two unsupported sleepers are spaced apart by 3 to 5 fully supported sleepers. An approach of a distributed model of the support for 2D simulations that uses Timoshenko beam element over an elastic foundation is shown in the paper [29]. The model, compared to the standard model with the 4-degrees Timoshenko element, contains analytically appended with additional degree of freedom of the vertical displacement. The improvement enhance the temporal response and avoiding rail stiffening and also corrects the overestimation of the contact force as well as reduce the computational costs.

An experimental investigation on the track-side estimating the sleeper support conditions is presented in [30]. The method is based on the inertial measurements on sleepers and the micro-tremor analysis to identity hanging sleepers. The interpretation of the relation between the longitudinal level and sampled micro-tremor using data is presented. An application of on-board inertial measurements from in-service trains for the identification of the sleeper support conditions is proposed in the research [31]. The GPS location measurements and carbody vertical accelerations were considered in a multi-resolution analysis and state machine design methodology for identification of the void zones. A diagnostic of the unsupported sleepers in transition zones using the photogrammetric method is presented in [32, 33, 34]. The study [32] demonstrates the results of a field monitoring study of a railway bridge transition with void defects using the measurement both track displacements using Digital Image Correlation and distributed rail strains using a Rayleigh-based fibre optic analyser. The measurements of rail–sleeper gaps are be used to obtain a first-order estimate of the shape of the differential track settlement profile. A similar photogrammetric method is presented in the experimental analysis [33] that was implemented in three transition zones in various conditions. it was found that the dynamic profile of the rail displacements has a good correlation with the track condition based on comparing the multiple-point displacements in the approaching zones in different conditions. An application of 3D DIC and pattern projection is proposed in [34] to assess the deformation of railway sleepers using on-board measurements. The full-field displacement and the crosstie's shape are measured. A resolution of approximately 5 microns is estimated to measure the relative tie deflections, both inside and outside the rail area. The time resolution was 100 frames per second. However, the used in the studies high-speed cameras with low time sampling rate could not fully reflect the dynamic interaction in void zones.

An analysis of the influence of parametric, periodic, and random excitation like wheel defects, hanging sleepers, and other periodic effects on the car-rail oscillatory sys-

 doi:10.20944/preprints202107.0066.v1

tem is presented in [35]. Experimental data on vibration parameters were determined using four inertial measurement units (IMU) installed on the axle boxes of the car running trolley wheel pairs. The signal spectra are analysed in relation to the defects.

A flexible track model in a multibody dynamics program is developed in the study [36] to simulate the influence of unsupported sleepers on ride comfort index. Field test on void zones is performed using LVDT sensors. Findings indicate that, in the case of a single unsupported sleeper through the track, the ride comfort index increased by 100% after increasing the train speed from 30 to 110 km/h. Field measurement tests and three-dimensional numerical analysis were conducted in the study [37] for pre-stressed concrete sleepers laid with different support. The experimental results show that the bending moment was increased more than three times due to the support conditions of the pre-stressed concrete sleepers and the rail roughness. Results of the numerical analyses show that the bending moment was increased more than two times because of the unsupported sleepers, and the tensile stress of the pre-stressed concrete sleeper exceeded 3 N/mm2 when the rail roughness was approximately 2 mm or more. Studying the effect of unsupported sleeper on dynamic characteristics of ballast beds using the DEM of a ballast bed is presented in [38]. The influence of unsupported sleepers and their number on the dynamic response of the ballast bed was analysed. The results show that the unsupported sleeper will redistribute the contact forces of ballast particles so that the number of strong force chains in the ballast will decrease, and the number of strong force chains in the adjacent ballast sleepers will increase.

Measurement of distributed rail strains on the track with unsupported sleepers using DIC and fiber optic sensing is presented in [39]. The measured rail strains were used to determine the rail shear forces and further load–deflection relationships for individual sleepers. The papers [40, 41] introduce a parallel co-simulation method to study vehicle-track dynamic interactions and their application for modelling the vehicle dynamics on a track with sleeper voids. The presented model is more than ten times faster than the conventional. The results show that the vertical rail deflections, wheel-rail contact forces and vehicle suspension forces are evidently larger for unsupported sleepers. A signal processing technique for evaluation of sleeper pseudo-deflection is presented in [42] to recover dynamic deflection of a railroad sleeper. The technique is based on a coupled measurement of acceleration and strain at the concrete sleeper. The developed method can be used for diagnostics of track support stiffness and identification of sleeper voids. An experimental investigation of track dynamic behavior in void zone is presented in [43]. It was found experimentally that the dynamic impact in time shift before the wheel reaches the impact zone. The numerical modelling confirmed and explained the phenomenon. Additionally, a simple method for the local track stiffness identification is proposed. An approach for track-side and on-board sleeper void identification and classification is proposed in the study [44]. The basic idea of the study lies on the especial pattern of dynamic impact in the void zone. The approach is based on machine learning methods that are improved by mechanical model. The data for the statistical models were acquired using DIC track-side measurements. Another recent techniques for the sleeper support condition estimation are based structural health monitoring (SHM) technologies such as smart or self-sensing sleepers as shown in the studies [45,46]. The information collected using embedded fiber Bragg grating sensing for tension measurements or acceleration sensors. The algorithms are developed to identify the condition indicators from raw measurements.

The literature review present a wide range of studies on numerical simulation of track and vehicle dynamic interaction considering unsupported sleepers. The numerical simulation is produced with help of different complexity models from simple beam models to detailed 3D FEM ones. However, most models serve as a simple imitation of experimental measurements without deep analysis of the interaction mechanics. The present experimental studies are not so numerous as the experimental ones and are limited to

Preprints (www.preprints.org) | NOT PEER-REVIEWED | Posted: 2 July 2021 doi:10.20944/preprints202107.0066.v1

some certain cases, mostly in transition zones. Therefore, the most models have pure experimental validation of the effects of the dynamic behavior in the zone of unsupported sleepers.

### 3. Experimental measurements and analysis of the void dynamic behaviour in a void zone

The previous research [43, 44] have shown that the dynamic behaviour of the track with voids is depending of many factors like void sizes, train loadings and velocities, axle distances etc. The studies considered the dynamic behaviour for the usual train loadings and velocities. However, the experimental studies indicate that the dynamic impact appear even for low velocities and light-weight vehicles. Thus, in the present study, the void dynamic behaviour for the case of low velocities and light-weight vehicles on the example of 2-axle Post wagon (Fig.3, top, left) of the Swiss Railways (SBB) is considered. The additional reason of the study case is that the vehicle axles have no influence on the neighbour ones that could simplify studying the mechanism of the dynamic impact.

The measurements we produced by SBB infrastructure departments [47] using high-speed video recordings, LVDT and acceleration measurements (Fig.3, top, right). A measurement of the rail deflection and the corresponding accelerations in a void zone for the post train with velocity 61 km/h is shown in Fig.3, bottom. The rail deflection line presents a locomotive and a series of the separate axle loading from post wagons. The maximal rail deflection 4 mm consists of elastic part about 0.5-1 mm and the void caused deflection about 3 mm. The diagram of accelerations presents quite different interaction behaviour: the maximal accelerations occur locally ant timely shifted to the maximal deflections. It indicates on an impact that occurs before the wheel reaches the sensor position and cause the maximal deflection of the rail. The impact appear only before the first locomotive axles and its amplitude is not much higher than the impacts from the post wagon axles.

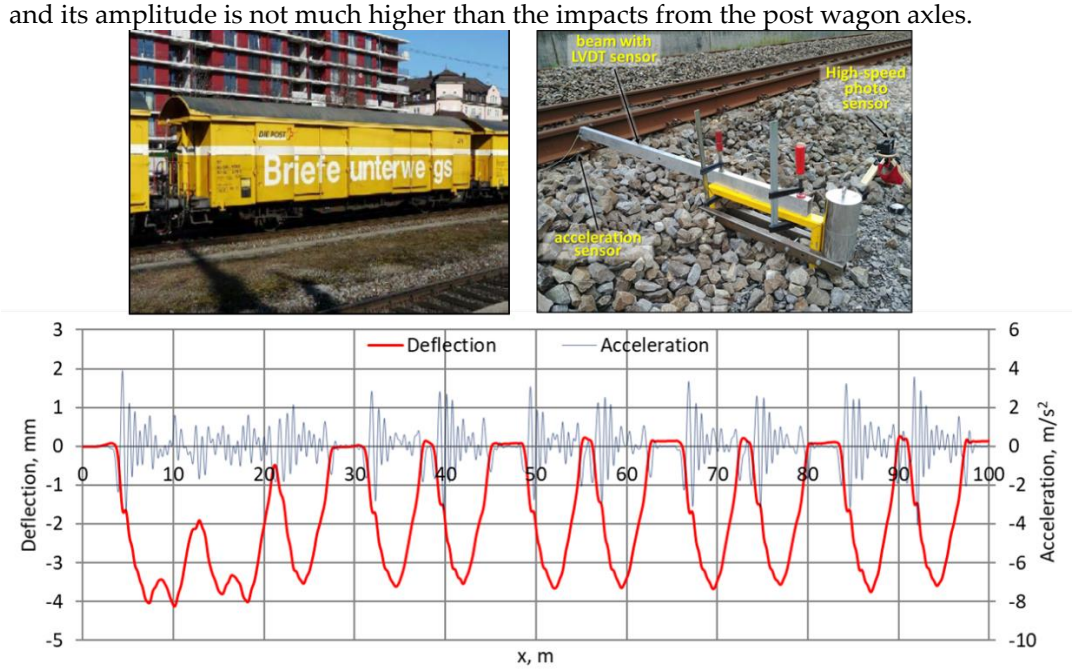


**Figure 3** Experimental measurement of track-side rail deflections (top, right) in the void zone for a slow light-weight post-train (top, left) and the measurement results (bottom)

The detailed analysis of the interaction for one axle is presented in Fig. 4. The deflection line has two special zones. The first one is about located under the first quarter of the deflection wave and the distance about 2 m to the maximal deflection point. The zone is characterized with the sudden appearance of oscillations that are damped until the wheel reaches sensor point. The oscillations are clear visible in the diagram of rail accelerations and also in the rail deflection line as a local disturbance. The first zone corresponds to the

Preprints (www.preprints.org) | NOT PEER-REVIEWED | Posted: 2 July 2021 doi:10.20944/preprints202107.0066.v1

dynamic interaction due to the void closing. A similar but lower distinct dynamic interaction appear during the right side of the deflection line that corresponds to the unloading part. The deflection line has a local disturbance that corresponds to the increase of acceleration that are about two times lower that in the first zone. The dynamic interaction in the second zones appear due to void opening while wheel leaving the void zone.

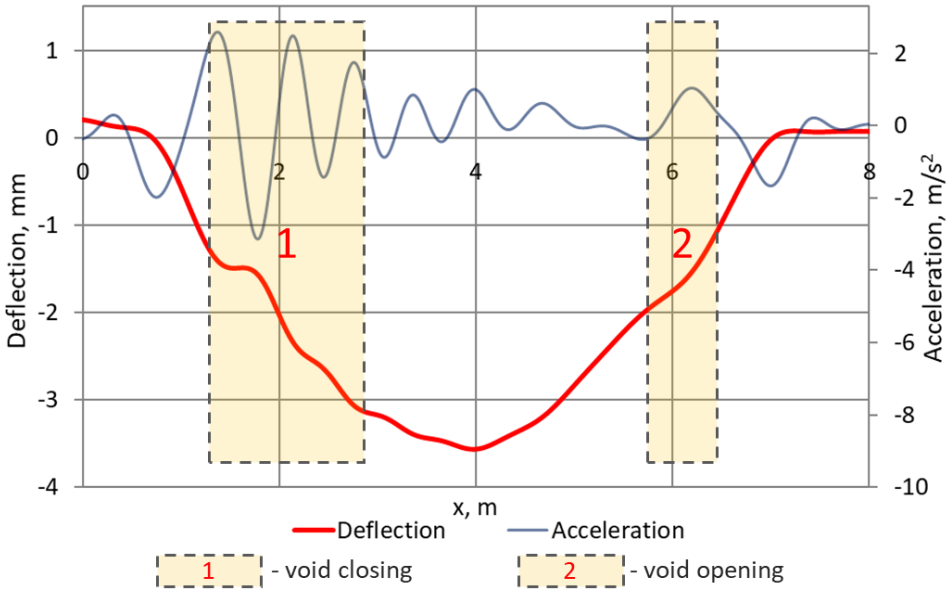


**Figure 4** The features of void in the rail settlement line

## 4. Numerical simulation of the dynamic impact

A numerical modelling is applied to explore the dynamic behaviour that observed from experimental measurements (Fig.3, Fig.4). The modeling is based on a 3 Euler-Bernoulli beam model that is coupled with two mass vehicle model (Fig. 5). The beams include the bending stiffness and masses. The beams are connected by continual layers that include the elasticity and damping and correspond to track elements: a rail, a sleeper with fastening, a ballast layer with a ballast bed. The void is taken into account as with help of the elasticity $k_2(x)$ and damping $\eta_{2(x)}$ properties of the layer between the second and the third beam over the void length $l_{\text{void}}$. The properties are bi-linear functions that provide the same elastic and damping parameters as in the outside zones after void closing. The more detailed description of the model is presented in the study [44], where the patterns of rail deflection and accelerations in the void zones are studied. The model parameters in the present study are selected to correspond to the post train from the experimental measurements. The track parameters are as follows: rail meter mass 60 kg/m, rail bending stiffness 6.4 MN·m², fastenings foundation coefficient 200 MN/m², fastenings damping 185 kN·s/m², sleeper meter mass 300 kg/m, sleeper layer bending stiffness 0.01 MN·m², sleeper-ballast foundation coefficient 600 MN/m², sleeper-ballast damping 75 kN·s/m², ballast meter mass 500 kg/m, ballast-subgrade foundation coefficient 200 MN/m², ballast-subgrade damping 680 kN·s/m². The vehicle parameters are as follows: car body mass for 1 wheel 7000 kg, unsprung wheel mass 400 kg, contact stiffness 2400 MN/m, contact damping 155 kNs/m, suspension stiffness $k_v$=0.6 MN/m, suspension damping 25 kNs/m.

Preprints (www.preprints.org) | NOT PEER-REVIEWED | Posted: 2 July 2021 doi:10.20944/preprints202107.0066.v1

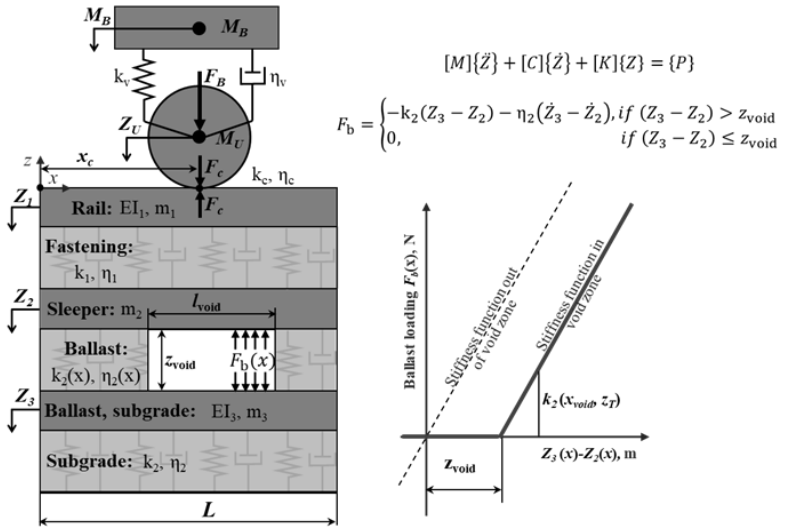


**Figure 5** The mechanical model of track and vehicle interaction in the void zone [44]

The present study, different to the previous studies [13, 44], is directed to the research of the sleeper-ballast interaction. The model parameters are fitted to the experimental measurement (Fig. 4). However not all parameters can be simply fitted, the void depth distribution along the track is not known as well as the sensor position relative to the void wave. Therefore, the void depth is considered as constant over the void length. However, to produce the plausible loading distribution, the both rectangular sides of the void wave are smoothed by flattened sinus function. Since the longitudinal location of the experimentally measured rail deflections (Fig. 4) is not known, multiple rail deflections are simulated with the step 0.5 m along the rail. The rail deflection simulation results that are presented in Fig. 6. Show similar to the experimentally measured deflections. The impact zone can be obviously recognised in the left side of the deflection line. The impact zone is differently shifted relative to the maximal deflection point depending on the track section. The right side if the deflection line has also a local disturbance zone due to void opening. Despite the similarities of the experimental and simulated results, there are differences in the overall deflection line. It is explained by non-constant void distribution along the track in the experimental case. The present paper aims studying the mechanism of the void impact appearing, therefore the constant void depth is assumed. The void depth distribution identification is a separate complicated problem that will be studied in the future research.

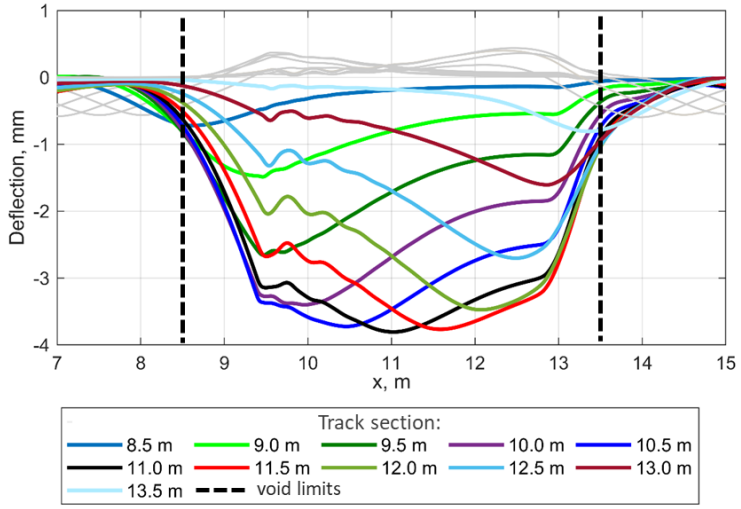


**Figure 6** The simulated rail deflections for the slow light-weight post-train in the rectangular form void

Preprints (www.preprints.org) | NOT PEER-REVIEWED | Posted: 2 July 2021 doi:10.20944/preprints202107.0066.v1

The Fig. 7 presents the track beams deflections, accelerations and loadings during the impact moment while the void is partially closed. It can be noted that the wheel position is shifted relative to the impact location. The sleeper acceleration in the impact point is more than two times higher than that of the rails. The loading diagram (Fig.7, bottom) shows the quasistatic loading distribution on the both sides of the void zone and the dynamic loading in the impact point.

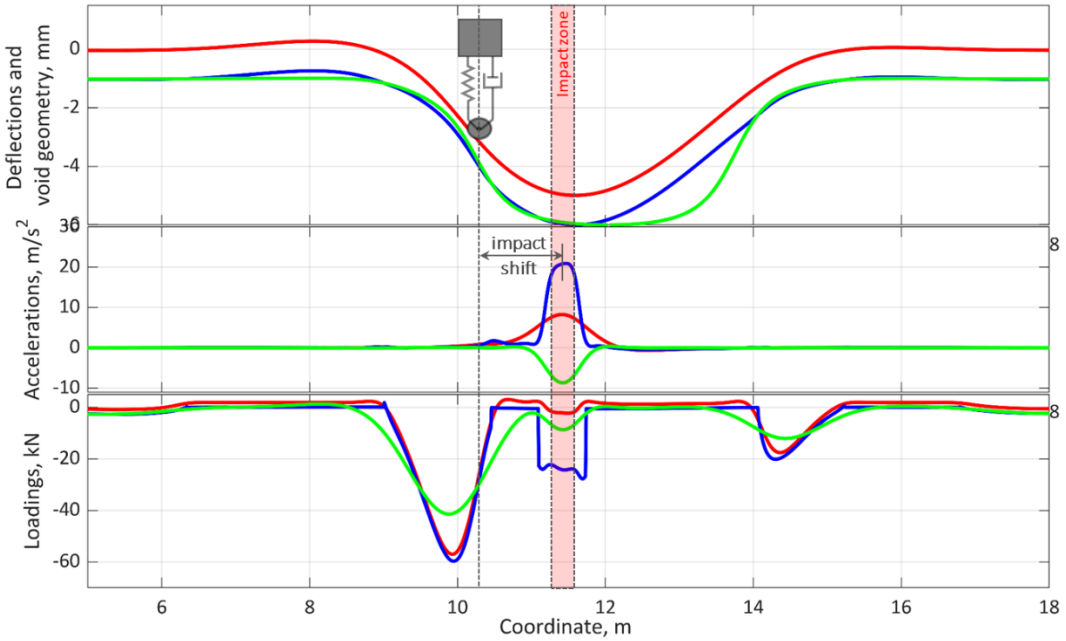


**Figure 7** Track loadings (bottom), accelerations (center) and deflections (top) along the track in the impact moment

The loadings of the ballast layer in the sections along the track that approximately correspond to the locations of the sleepers in the void zone are presented in Fig. 8. Notable is the impact loading in the section 10.5 m that is detailed depicted in the bottom diagram. The loading consists of the short impact part with about 30 kN maximal value and the following quasistatic part with about the same maximal value. Before the impact, the ballast was fully unloaded. The ballast loadings on the another sections have less notable impact part but very distinct quasistatic one. The neighbour sections to the void zone 9.5m and 13.5m are more loaded than the ballast outside the void zone but have also high initial preloading. The similar loading property in the track sections inside the void zone is the absence of the preloading.

Preprints (www.preprints.org) | NOT PEER-REVIEWED | Posted: 2 July 2021 doi:10.20944/preprints202107.0066.v1

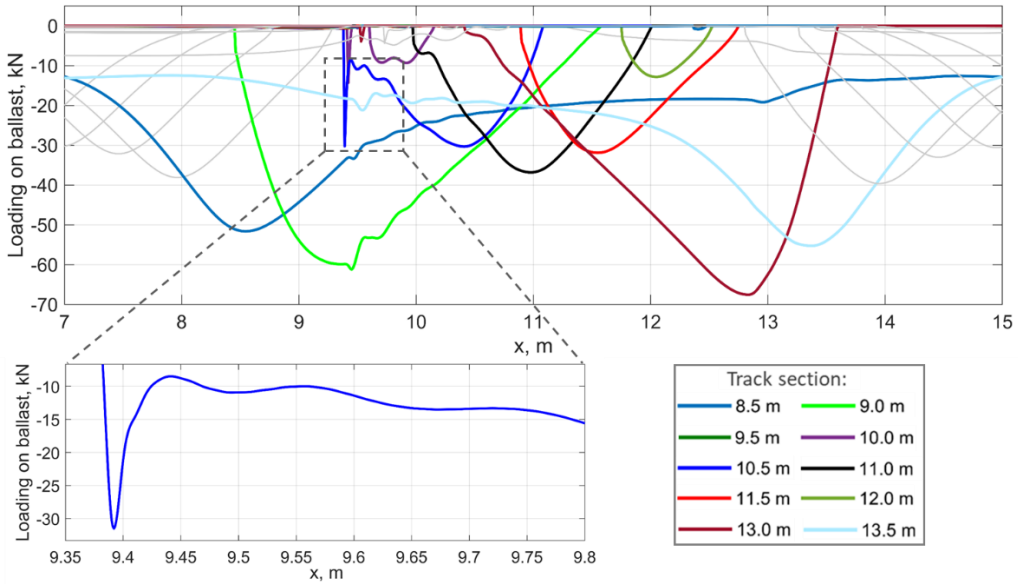


**Figure 8** Loading of the sleepers to the ballast and the highlighted impact loading

The sleeper and wheel acceleration are presented in Fig. 9. While the sleeper accelerations reach 30 m/s2, the maximal wheel acceleration is about 10 m/s2. Two acceleration zones are visible – for the void closing and opening. The maximal wheel acceleration is shifted in time relative to the maximal acceleration of the sleepers.

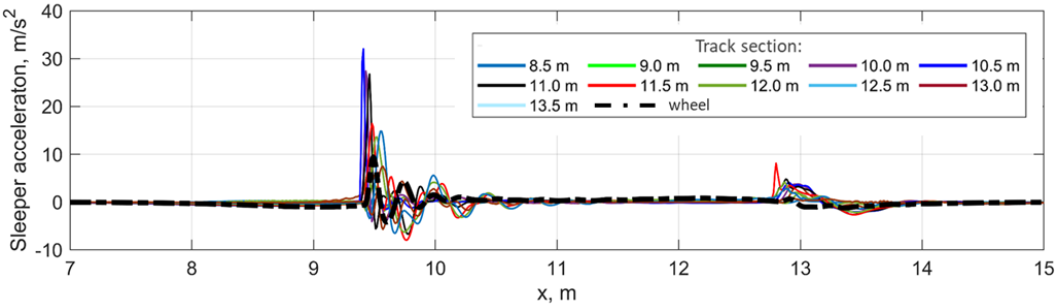


**Figure 9** Sleeper and wheel accelerations

Additionally to the accelerations, the vertical velocities of the wheel and the sleepers is another important parameter that can explain the mechanism of the void impact. The diagram of the wheel and sleeper velocities is presented in Fig. 10. The diagram shows that the wheel and the sleepers in the void zone move together with the same vertical velocity until the impact time. After that, the sleepers quick decrease the velocity and the wheel change its velocity gradually to the reverse.

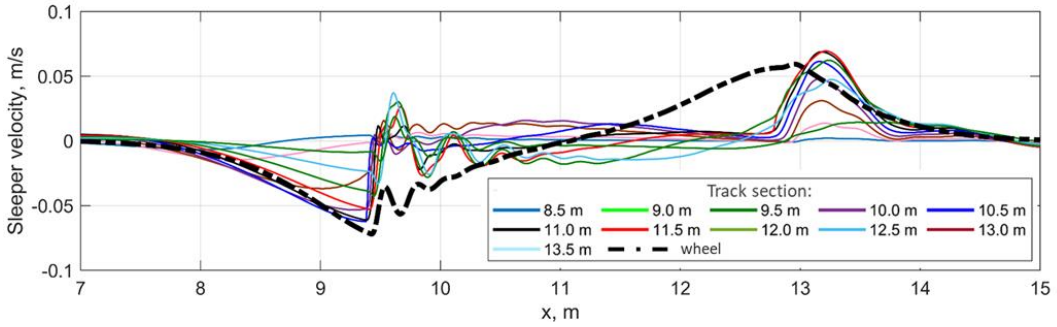


**Figure 10** Sleeper and wheel velocities

Preprints (www.preprints.org) | NOT PEER-REVIEWED | Posted: 2 July 2021 doi:10.20944/preprints202107.0066.v1

## 5. Analysis of the influence of the sleeper and void size on impact loading, acceleration and velocity

Different to a geometrical irregularity, the influence of the void depth on the dynamic interaction is ambiguous i.e. until some depth the loadings increase and after it should decrease until full unloading. The same is valid for the void length: for the short voids, the deflections and thus the impacts decrease. The aim of the section is a quantitate study of relations between the void sizes and the parameters of the dynamic interaction. The following parameters are analyzed: wheel and sleeper maximal accelerations, sleeper impact velocity, impact loading and quasistatic (QS) loadings. The QS loadings are considered in the void zone and outside the void zone. Additionally, the impact shift or the distance between the maximal impact time and that of QS loading from the same track location. The calculation cases are named with the labels Lxvx denoting the theoretical length and depth. The actual void sizes result after the gravitational loading and therefore the values are 25-50% lover that the labelled. Thereby, the calculations cases for the short voids are limited those where the void is closed and the dynamic impact appeared. The same is considered for the long void zones where the void is closed under the own weight of the sleepers and rails. The results of the variate calculations are presented in the Table 1.

**Table 1** Impact simulation results

| Case | Sleeper | | Impact shift, m | Wheel acceleration, m/s² | Ballast | | | Rail deflection | | Void | |
|---|---|---|---|---|---|---|---|---|---|---|---|
| | Impact velocity, cm/s | Max acceleration, m/s² | | | Impact loading, kN | QS loading in void zone, kN | QS loading outside void zone, kN | negative, mm | positive, mm | Void length, m | Void depth, mm |
| L2V1 | 1,4 | 4,9 | 0,24 | 1,1 | 5,44 | 6,21 | 52,1 | 1,01 | 0,1 | 1,4 | 0,85 |
| L2V2 | 1,4 | 0,86 | - | 0,82 | 0 | 0 | 59,4 | 1,23 | 0,1 | 1,49 | 1,84 |
| L3V1 | 1,6 | 2,64 | 0,56 | 0,36 | 3 | 23 | 51,6 | 1,1 | 0,1 | 1,93 | 0,75 |
| L3V2 | 2,3 | 6,65 | 0,28 | 3,02 | 2,94 | 10,82 | 61,13 | 1,83 | 0,1 | 2,05 | 1,671 |
| L3V3 | 2,0 | 1,24 | - | 1,24 | 0 | 0 | 65,8 | 2,16 | 0,13 | 2,2 | 2,65 |
| L4V1 | 3,4 | 4,26 | - | 0,12 | 1 | 27,88 | 47,36 | 0,97 | 0,15 | 2,4 | 0,53 |
| L4V2 | 1,6 | 12,51 | 0,63 | 2,6 | 10,01 | 22,45 | 58,78 | 1,77 | 0,16 | 2,58 | 1,42 |
| L4V3 | 2,7 | 15 | 0,35 | 5,52 | 16,5 | 14,65 | 64,18 | 2,6 | 0,16 | 2,77 | 2,36 |
| L4V4 | 3,2 | 3,52 | | 2,73 | 0 | 0 | 67,54 | 3,29 | 0,16 | 2,94 | 3,31 |
| L5V1 | 3,1 | 5,86 | 1,25 | 0,034 | 4,55 | 28,63 | 43,77 | 0,88 | 0,12 | 2,78 | 0,26 |
| L5V2 | 1,3 | 13,16 | 0,87 | 1,5 | 11,77 | 24,6 | 54,49 | 1,66 | 0,19 | 3,07 | 1,08 |
| L5V3 | 2,7 | 23,24 | 0,64 | 6,02 | 22,04 | 29,8 | 60,8 | 2,38 | 0,24 | 3,27 | 1,97 |
| L5V4 | 3,9 | 19,66 | 0,38 | 7,9 | 20,56 | 25,77 | 64,64 | 3,14 | 0,38 | 3,44 | 2,87 |
| L5V5 | 4,5 | 5,23 | 0,41 | 11,04 | 4,49 | 17,38 | 67,52 | 4,31 | 0,37 | 3,5 | 4,26 |
| L6V1 | 4,0 | 4,42 | 1 | 0,13 | 4,35 | 33,23 | 40,83 | 0,61 | 0,15 | 3,23 | 0,25 |
| L6V2 | 0,9 | 9,96 | 1,02 | 1,09 | 9,33 | 33,74 | 49,86 | 1,07 | 0,39 | 3,57 | 0,8 |
| L6V3 | 2,3 | 19,79 | 1,24 | 3,9 | 16,08 | 33,21 | 56,39 | 1,87 | 0,35 | 3,74 | 1,46 |
| L6V4 | 3,7 | 27,15 | 1,08 | 7,6 | 20,71 | 31,76 | 60,33 | 2,76 | 0,29 | 3,87 | 2,31 |
| L6V5 | 4,9 | 29,72 | 0,87 | 9,95 | 21,8 | 29,72 | 63,14 | 3,69 | 0,23 | 4,04 | 3,2 |
| L6V6 | 5,8 | 31,58 | 0,76 | 11,02 | 28,54 | 26,25 | 64,86 | 4,6 | 0,17 | 4,11 | 4,18 |
| L6V7 | 6,0 | 30,95 | 0,56 | 11,15 | 29,1 | 22,61 | 65,79 | 5,49 | 0,1 | 4,18 | 4,99 |

Preprints (www.preprints.org) | NOT PEER-REVIEWED | Posted: 2 July 2021 doi:10.20944/preprints202107.0066.v1

| | | | | | | | | | | | |
|---|---|---|---|---|---|---|---|---|---|---|---|
| L7V2 | 5,7 | 10,28 | 1,3 | 0,72 | 9,67 | 24,78 | 45,41 | 0,74 | 0,34 | 3,95 | 0,14 |
| L7V3 | 1,7 | 19,2 | 1,46 | 2,36 | 18,14 | 33,35 | 52,43 | 1,64 | 0,1 | 4,16 | 0,86 |
| L7V4 | 3,1 | 23,07 | 1,25 | 4,93 | 23,22 | 37,12 | 56,17 | 2,54 | 0,1 | 4,34 | 1,63 |
| L7V5 | 4,5 | 32,1 | 1,55 | 9,42 | 30,27 | 36,71 | 59,87 | 3,82 | 0,1 | 4,51 | 2,86 |
| L7V6 | 6,1 | 38,14 | 0,99 | 10,65 | 37,75 | 36,4 | 60,84 | 4,24 | 0,1 | 4,6 | 3,29 |
| L7V7 | 6,6 | 48,1 | 0,76 | 12,81 | 46,05 | 35,74 | 62,36 | 5,08 | 0,1 | 4,69 | 4,15 |
| L7V8 | 7,3 | 45,82 | 1,29 | 13,34 | 43,86 | 34,27 | 63,16 | 5,89 | 0,1 | 4,7 | 5,03 |

The diagrams of the maximal wheel and sleeper accelerations for all length cases are presented in Fig.11. Remarkable is almost four times higher sleeper acceleration than the wheel one. The further notable property of the both acceleration processes is the gradual stabilization of the accelerations with the increased void depth. Moreover, the acceleration decrease for the short void cases L2-L5 together with the increase of the void depth. The long void cases L6-L7 show almost no change of the accelerations for more than 4 mm void depth.

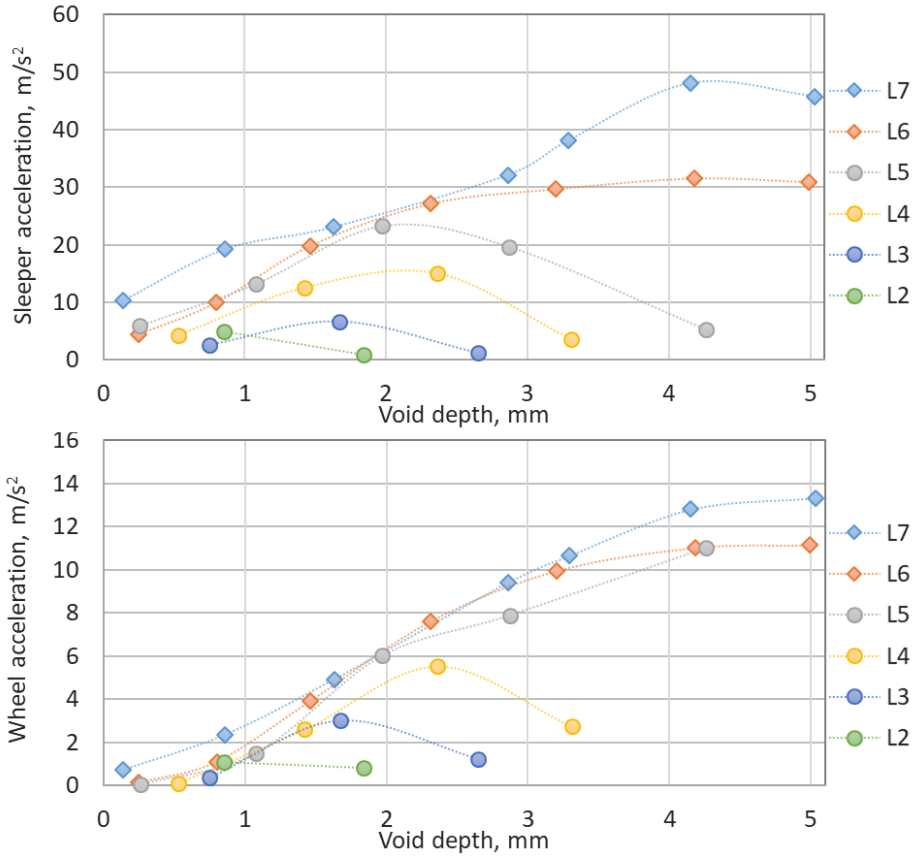


**Figure 11** Relation of the wheel and sleeper acceleration to the void depth

The ballast impact loading process that is presented in the Fig. 12 is similar to the sleeper acceleration one (Fig. 11). However, the impact loading is absent for the cases L2-L4 and high depth. Both the diagram of the impact accelerations and the loadings have some non-monotonous parts that can be explained with the selected track longitudinal sectioning each 0.5m. The short impact time could cause that the maximal impact position could be located between the selected raster. The maximal impact loading is for the cale L7v7 that corresponds to the void length 4.7m and the depth 4.2mm.

Preprints (www.preprints.org) | NOT PEER-REVIEWED | Posted: 2 July 2021 doi:10.20944/preprints202107.0066.v1

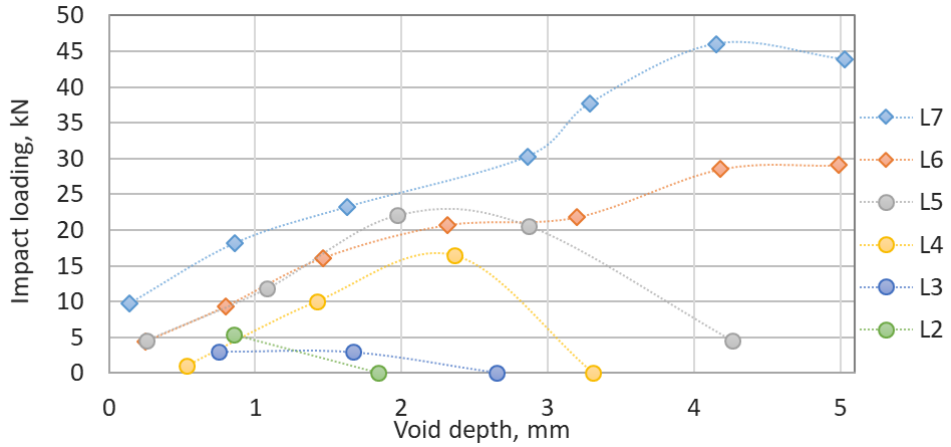


**Figure 12** Relation of the impact loading to the void depth

The analysis of the quasistatic loadings inside the void zone and outside of it is presented in Fig.13. The quasistatic loadings outside the void zone (Fig. 13, bottom) present clear relation to the void depth – the loadings increase up to 17kN while the void depth growing up to about 2mm. The influence of the void length is minor. However, the short void cases with the highest void depth generally cause higher load distribution on the void ends.

The quasistatic loadings inside the void zone present an ambiguous relation to the void sizes. The sleeper loading for the long void zones L7 is about the same as for the track without voids. However, in case of the short void zones L2-L3, the quasistatic loading decrease rapidly while the void depth increases. The quasistatic loadings inside the void zone is absent for the void lengths less than 3 m with the depths more than 3.3mm

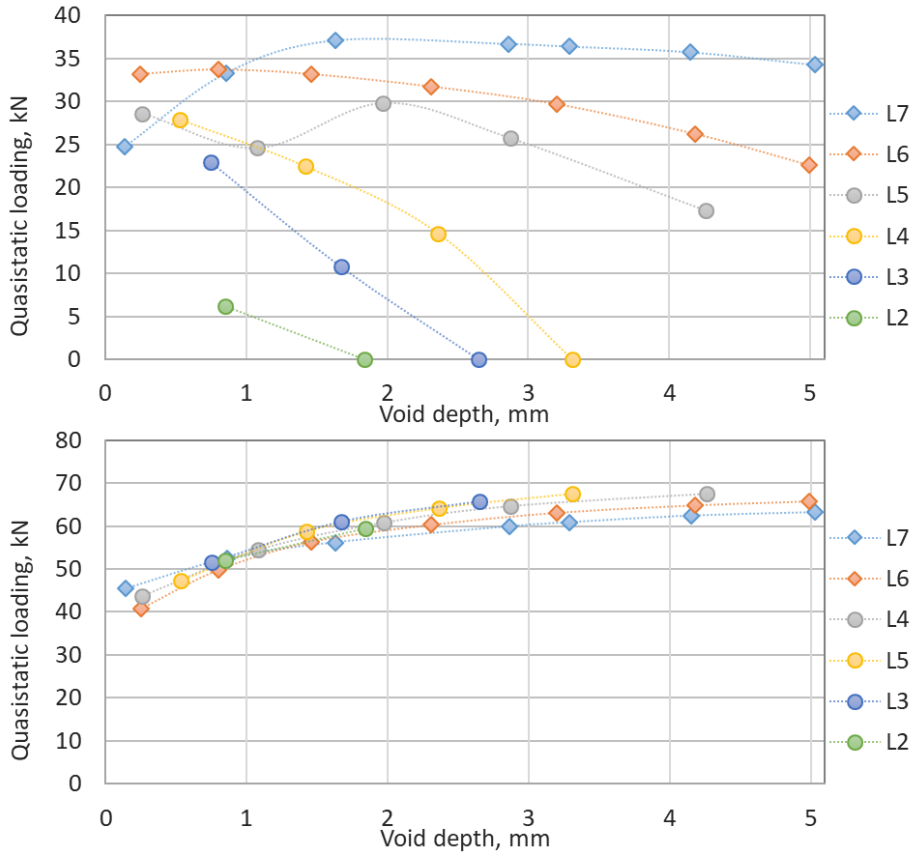


**Figure 13** Relation of the quasistatic loading to the void depth inside the void zone (top) and outside the void zone (bottom)

Preprints (www.preprints.org) | NOT PEER-REVIEWED | Posted: 2 July 2021 doi:10.20944/preprints202107.0066.v1

## 6. Analytic explanation of the void impact mechanism

The analysis of modelling results in the previous section has shown that the dynamics due to the wheel passing the void zone is relative low to that in the sleeper-ballast contact. Additionally, different to the geometrical irregularities, there is some void depth with the maximal impact interaction. Thus, the main reason of the impact interaction is not the wheel-track oscillations due to the appearing irregularity. A void impact explanation due to quasistatic void closure is proved in the study. The impact velocity is derived from a simple clamped beam elastic line with moving point loading of the wheel that is presented on Fig. 14. The diagrams present the shear loadings, moment and the beam deflections. The maximal deflection of the beam $f_{max}$ hast its coordinate $x_{max}$ while the point loading $F$ coordinate is $a$.

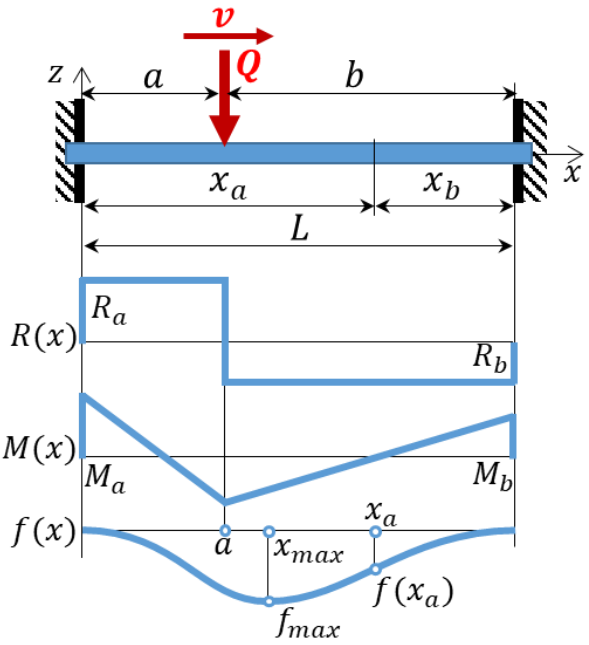


**Figure 14** Static scheme for determining a track deflection in a void zone

The governing equations that correspond to the Fig.14 are presented by formulas (1-6) [55-56]. The loading reactions $R_a$ and $R_b$ in the clamp points are determined using the following equations:

$$R_a = Q \cdot (3a + b)\frac{b^2}{L^3}\,, \tag{1}$$

$$R_b = Q \cdot (a + 3b)\frac{a^2}{L^3}\,, \tag{2}$$

where, Q – point loading; $a, b$ – coordinates of the point loading from both beam sides; $L$ – beam length.

The clamp moments reactions $M_a$ and $M_b$ are determined as follows:

$$M_a = -Q \cdot a \cdot \frac{b^2}{L^2}\,, \tag{3}$$

$$M_b = -Q \cdot b \cdot \frac{a^2}{L^2}\,. \tag{4}$$

The elastic beam deflections in the range from the clamps $0 \le x_a \le a$ and $0 \le x_b \le b$ to the impact point location are determined by formulas:

$$f_1(x_a) = M_a \cdot \frac{x_a^2}{2EI} + R_a \cdot \frac{x_a^3}{6EI}\,, \tag{5}$$

$$f_2(x_b) = M_b \cdot \frac{x_b^2}{2EI} + R_b \cdot \frac{x_b^3}{6EI}\,, \tag{6}$$

where, $EI$ – bending stiffness.

Preprints (www.preprints.org) | NOT PEER-REVIEWED | Posted: 2 July 2021 doi:10.20944/preprints202107.0066.v1

Additionally, a clamped beam deflection due to own weight is taken into account using the formula

$$f_w(x_a) = -q \cdot L^2 \cdot \frac{x_a^2}{24EI} \cdot \left(1 - \frac{x_a}{L}\right)^2, \tag{7}$$

where, $q$ – distributed loading of own weight of the sleepers and rails.

The maximal beam deflection is found using the formula (6) of the right side of the beam, assuming that the loading position is located on the left-side. The corresponding equation without own weight deflection is as follows:

$$\frac{df_2(x_b)}{dx_b} = \frac{Q \cdot a^2 x_b^2 \cdot (a + 3b)}{2EI \cdot L^3} - \frac{Q \cdot a^2 \cdot b \cdot x_b}{EI \cdot L^2} = 0 \tag{8}$$

The solution and simplification of the equation delivers the coordinates of the impact point and the maximal deflection depending on the loading position $a$:

$$x_{max}(a) = L - \frac{2L \cdot (L - a)}{3L - 2a} \tag{9}$$

$$f_{max}(a) = -\frac{2Q \cdot a^2 \cdot (L - a)^3}{3EI \cdot (3L - 2a)^2} \tag{10}$$

The resulting relations (9, 10) are simple but they do not take into account the variable beam deflection $f_w(x_a)$ due to own weight. The analytical solution of the equation (8) with the own weight part is possible, however it is complicated that is not plausible for the aim of analytics. An assumption that the weight deflection is constant, equal to its maximal value and not dependent to the variable $x_b$, provides an approximate solution that is exact enough for practical calculations. The Fig. 15 shows the comparison of the exact and approximate solutions. The deviation of the maximal value coordinate is about 8%, but the deviation of the maximal values is less than 1%.

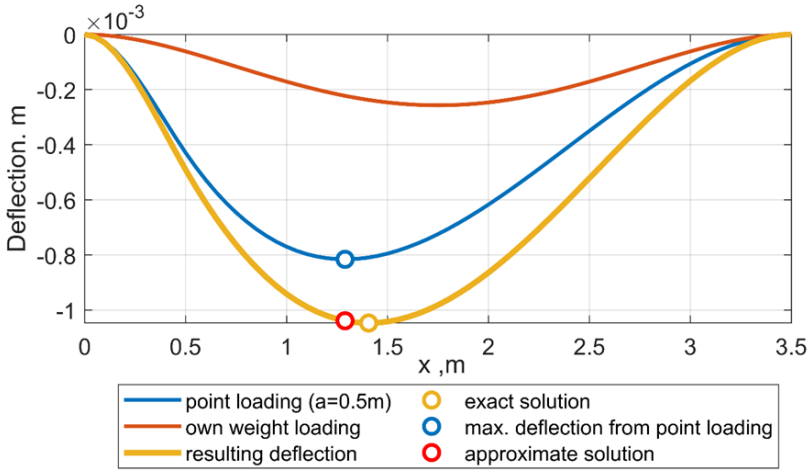


**Figure 15** Rail deflection line for wheel point loading case with the dustributed own weight loading and the maximal deflection using exact and approximate solution

The derived formula (10) explains the relation of the maximal beam deflection to the loading position. However, to determine the impact velocity for known void depth, the wheel position identification $a$ that corresponds to void depth $V$ is necessary. Thus the equation for the solution is:

$$f_{max}(a) = V. \tag{11}$$

The exact solution of the equation (1) is not possible due to derivation of the 5th degree polynomials. However, assuming that the wheel position $a$ is usually up to 0.6m a

Preprints (www.preprints.org) | NOT PEER-REVIEWED | Posted: 2 July 2021 doi:10.20944/preprints202107.0066.v1

simplified analytic relation can be found that provides less than 5% error compared to the exact solution:

$$a_V = \frac{27L\left(18EI{\cdot}V + \sqrt{2}Q{\cdot}\sqrt{\left(\frac{EI{\cdot}V}{Q(3L-1)^3}\right)}\ (27L^2 - 27L^3 - 9L)\right)}{2(-27Q{\cdot}L^3 + 27Q{\cdot}L^2 - 9Q{\cdot}L + Q + 162EI{\cdot}V)}. \quad (12)$$

The vertical impact velocity of the beam is determined assuming the constant velocity of the loading point $a(t) = v \cdot t$ along the beam and differentiation of the equation (10):

$$V_{imp}(t) = \frac{df_{max}(v{\cdot}t)}{dt} = \frac{d}{dt}\left(\frac{2Q{\cdot}t^2{\cdot}v^2{\cdot}(L - t{\cdot}v)^3}{3EI{\cdot}(3L - 2t{\cdot}v)^2}\right), \quad (14)$$

The resulting formula of impact velocity depending on the wheel position and its velocity is following.

$$V_{imp}(a) = \frac{2{\cdot}Q{\cdot}a{\cdot}v{\cdot}(L-a)^2{\cdot}(2{\cdot}L^2 - 5{\cdot}L{\cdot}a + 2{\cdot}a^2)}{EI{\cdot}(3{\cdot}L - 2{\cdot}a)^3}. \quad (15)$$

The analysis of the equation shows that the impact velocity depends linear to the wheel velocity, different to the geometrical irregularities where the relation is quadratic. Additionally, it can explain why the low-speed trains also cause the significant impacts in the void zones. The relation of the impact velocity to the wheel loading $Q$ is linear. However, the loading $Q$ includes both static and dynamic parts that for short irregularities would cause the dynamic effects.

The relation of the impact velocity to the void depth is explained by formulas (12) and (15) together. However, the influence is complicated and not clear. The diagram on the Fig.16 shows the relation of the impact velocity the void depth for different void length cases. The beam bending stiffness and the loading are the same as for the simulation in the Section 2. The void mean lengths and their minimal and maximal values are taken from the table 1 to provide better comparison to the simulation results. The diagram shows that there is a maximal impact velocity for the certain void depth and for each void length. The maximal impact velocity is up to 7cm/s for the case L7.

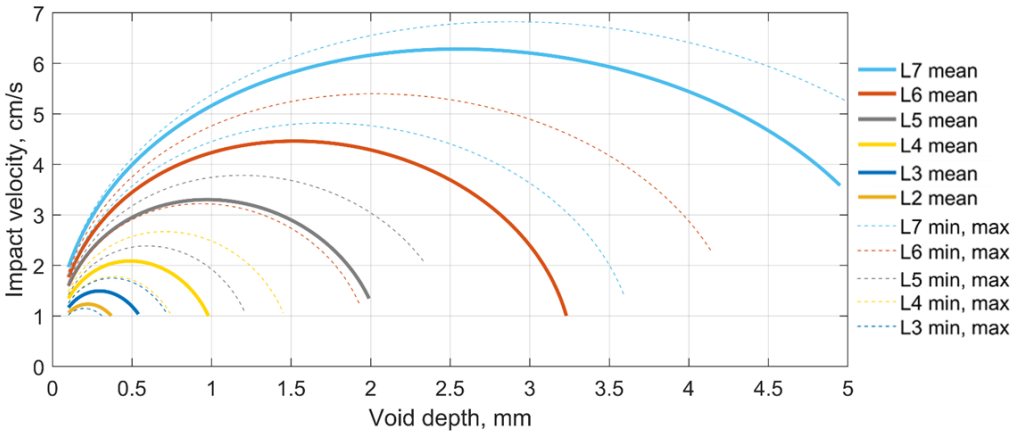


**Figure 16** Quasistatic relation of the sleeper impact velocity to the void depth

The results are compared with the simulated sleeper impact velocity relation to the depth that is presents in the Fig. 17. The diagrams in the both figures present the similarities: the impact velocity is in about the same range, the maximal impact velocities are observed. However, the maxima are shifted to the right side. The explanation of the difference is that the both diagrams cannot be directly compared. Each void depth point on

Preprints (www.preprints.org) | NOT PEER-REVIEWED | Posted: 2 July 2021 doi:10.20944/preprints202107.0066.v1

the diagram Fig.17 correspond to the different void length from the Table 1, whereas the lines on the diagram Fig.16 have a constant void length and higher void length is usually result in higher impact velocity. Moreover, high void sizes cause the growing dynamic effect of wheel and rail interaction.

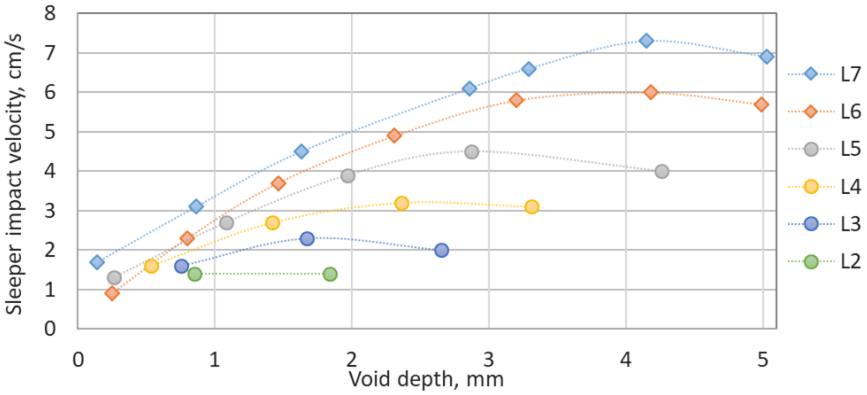


**Figure 17** Relation of the sleeper impact velocity to the void depth

## 7. Estimation of residual settlement intensity of the ballast layer in the void zone

The aim of the section is an estimation of the long-term influences of the ballast loading in the void zone. The DEM is widely used to study the ballasted track of railway [57-62]. Jing et al. [63] used the DEM to simulate the hanging sleeper dynamic characteristics of ballast bed, and the ballast particle breakage under dynamic cyclic loads was investigated. Thus, the estimation in this study is produced using a DEM algorithm to simulate residual settlements of one sleeper in a ballast box (Fig. 18, top) under the dynamic loadings of the different cases. The sleeper geometry corresponds to B70 sleeper. The particles form is simple balls with the size standard distribution 22.5-63mm. The model mechanical parameters we derived with the model calibration to the accurate model with the natural form particles [64, 65]. Thus, the used model is dimension reduced one having the advantage of quick simulation that is important for the simulation the settlement accumulation requiring many loading cycles to receive the definite settlement intensities. The number of the particles is 29788. The particle material properties are the following: static friction 0.56, dynamic friction 0.54, restitution coefficient 0.72, bulk density 1700 kg/m3, Young Modulus 50 GPa, Poisson ratio 0.3, rolling resistance 0.38. The sleeper and the subgrade properties are the following: static friction 0.56, dynamic friction 0.54, restitution coefficient 0.72, density 2650 kg/m3, Young Modulus 20 GPa, Poisson ratio 0.3. The rolling resistance model corresponds to the elastic-plastic approach [48] that takes into account rolling radii, the tangential stiffness, rolling resistance coefficient etc. The tangential force model is a simple elastic Coulomb model. The normal force model is a linear hysteresis one.

Preprints (www.preprints.org) | NOT PEER-REVIEWED | Posted: 2 July 2021 doi:10.20944/preprints202107.0066.v1

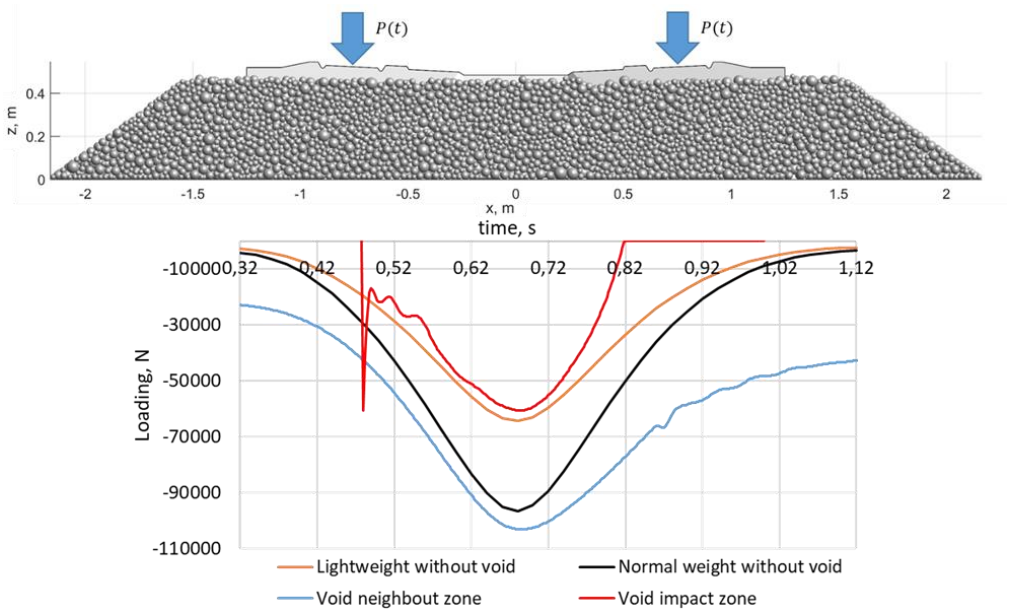


**Figure 18** The DEM model geometry (top) and the loading cycles for the loading cases (bottom)

Four different cases of the ballast dynamic are considered: normal weight wagon (100kN/wheel) for the track without void and light weight wagon for the track without void, pre-stress and quasistatic loading in the neighbour zones and high impact inside the void. The first loading cycles for the DEM simulation are presented in Fig. 18, bottom. The impact loading case in the void zone (red line) consists of the short time impact and long quasistatic part without the own weight pre-stress. The neighbour to the void zone (blue line) is characterised with high pre-stress and higher ballast loading than in case of normal weight car on the track without void.

Before the modelling the model particles were fully stabilised to provide possibly low non-stationary initial settlement. However, the all simulation results had some accelerated initial settlements. Therefore, the modelling was produced in 600 loading cycles, but for the analysis was use the end linear part with 400 cycles. The residuals settlements are estimated using the upper envelope line of the sleeper deflections that corresponds to the ballast unloaded state. The results of the residual settlements for the loading cycles are presented in Fig. 19. The results show, that the settlement intensity for the lightweight trains and the track without voids is about 0.72 mm/Mio axles and the same for the normal weight car is 2.27 mm/Mio axles. Thus, the settlement intensity increases more than 3 times for the increase of the maximal loading about 57%. The result does not contradict to the relative empirical estimations of the ORE C161 [49] and the AASHO Road Test [50]. Moreover, the results have a good agreement with the experimental studies [51, 52].

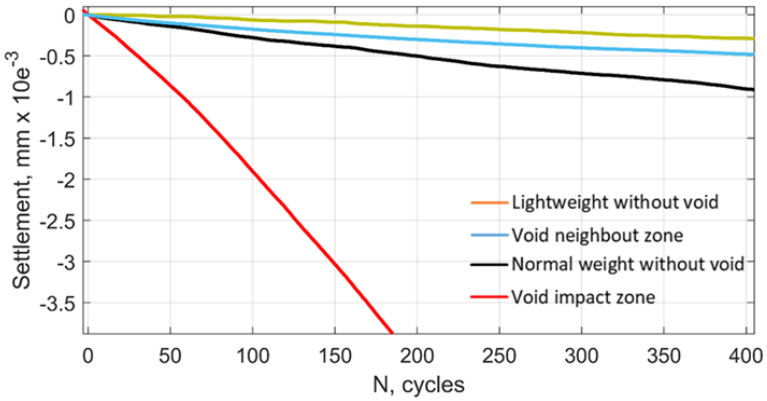


**Figure 19** Residual settlement lines for the loading cases

Preprints (www.preprints.org) | NOT PEER-REVIEWED | Posted: 2 July 2021 doi:10.20944/preprints202107.0066.v1

The loading case for the lightweight rolling stock and the pre-stresses ballast on the both sides of the void zone (Fig. 19, blue) shows the similar settlement intensity as for the loading without void. However, the line has a long initial stabilisation phase, that usually appear because of a sudden increase of the loading. The similar intensity can be explained with the similar amplitude of the dynamic part of the loading. The settlement line for the void impact zone is quite outstanding form the other settlement cases. The settlement intensity is more than 8 times higher than for the normal weight case despite lower loading maxima. Moreover, the settlement intensity seems to have some acceleration of the intensity. The present studies on the influence of the dynamic loadings [2, 53] show wide range of the possible intensities with the maximal ones much higher than the present settlement intensity. However, the real cause of the intensity increase is not obvious due to unknown influence of the full unloading state. The influence of the both factors is the aim of the further studies.

To explain the quick ballast settlements, the intermediate reasons are considered based on the analysis of the internal processes in the ballast layer, namely loading distribution from the sleeper to the subgrade. The Fig. 20 presents the maximal normal loading distribution in the ballast particles for one moment after full load cycles for two cases: the impact loading (Fig. 20, top) and the high pre-stressed state of neighbour zone (Fig. 20, bottom). The particles are visualised in both transparency and colour from blue to red depending on the acting normal force. The particles with the normal force less than 5% of the maximal value are not visualised. The red zones of the particles could be interpreted as a good loading transmission from the sleeper to the subgrade. The normal force distribution for the impact case present clear differences to the normal case under the sleeper ends: the number of high loaded particles for the impact case is lower.

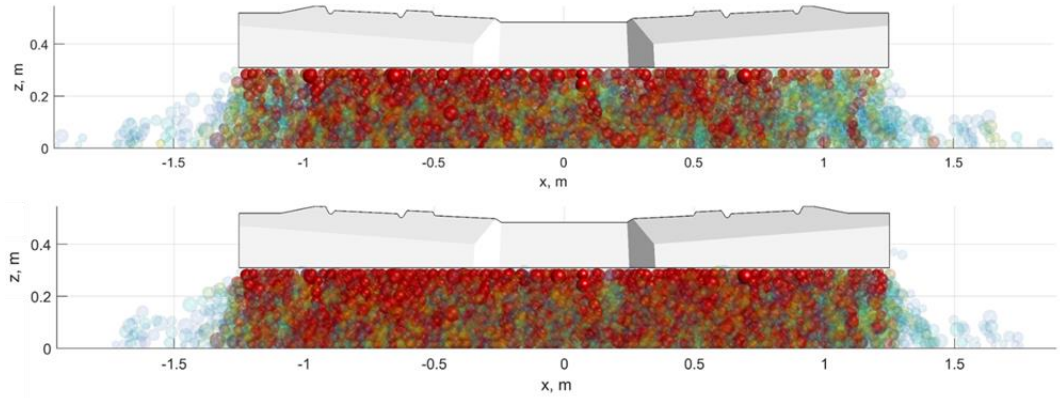


**Figure 20** The distribution of the normal force over the particles after impact loading series (top) and after the quasistatic cyclic loading (bottom)

An analysis of the loading distribution along the sleeper is performed to produce a quantified estimation of the loading transmission from the sleeper to the subgrade. The Fig. 21 presents the normal loading distribution in the particles and its mean value along the sleeper x-axis for the zones under the sleeper (top) and over the subgrade (bottom). The mean normal loading diagrams are characterised with 3 zones:

- the good supported mean part of the sleeper with the mean loading about 205 N/particle under the sleeper and about 127 N/particle over the subgrade;
- the sleeper sides 0.25-0.5m with the particle loading breakdown to 145-162 N/particle under the sleeper and about 94-101 N/particle over the subgrade;
- zones outside the sleeper that carry not more than 10% of the loading.

The loading breakdown under the sleeper ends is about 30% lower than that on the stable zone. The property of the ballast layer to carry, transmit and distribute the loading from the sleeper to the subgrade can be estimated with the particle loading ratio in the

Preprints (www.preprints.org) | NOT PEER-REVIEWED | Posted: 2 July 2021 doi:10.20944/preprints202107.0066.v1

stable zones under the sleeper and over the subgrade. The parameter loading transmission is 1.61 for the cyclic loading case with low settlement intensity.

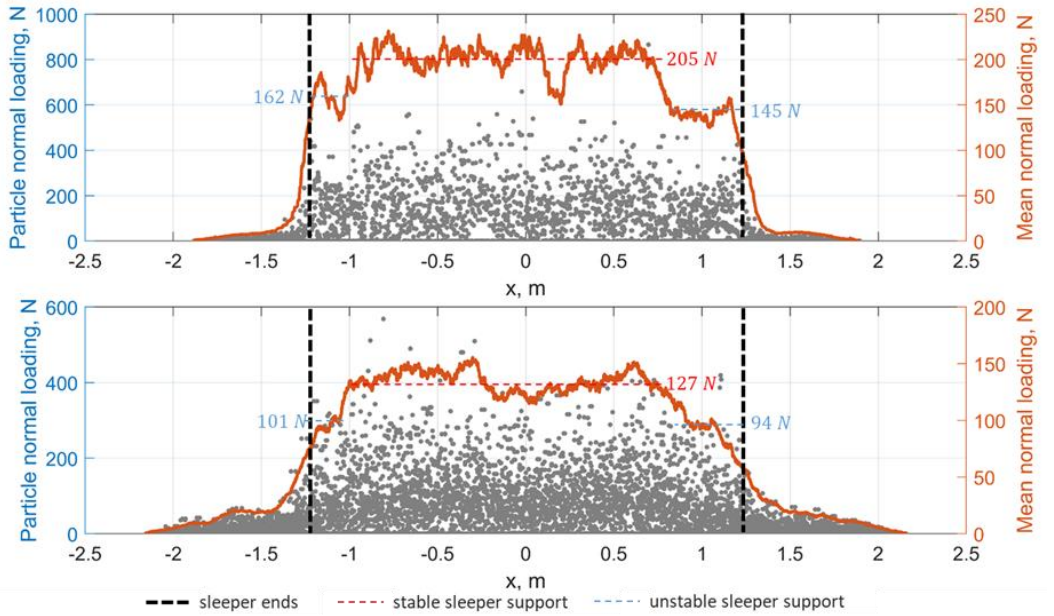


**Figure 21** The mean normal loading distribution in the particles under the sleeper (top) and over the subgrade (bottom) after the quasistatic loading cycles

The analysis of the particle loading distribution for the impact case in Fig. 22 shows the different distribution to the quasistatic cyclic loading. Notable are the breakdown zones under the sleeper ends with the mean particle loadings 72-87N/particle under the sleeper and 49-63N/particle over the subgrade. Thus, the loading breakdown is up to 50%. The parameter loading transmission is 1.33 for the impact loading case with the high settlement intensity.

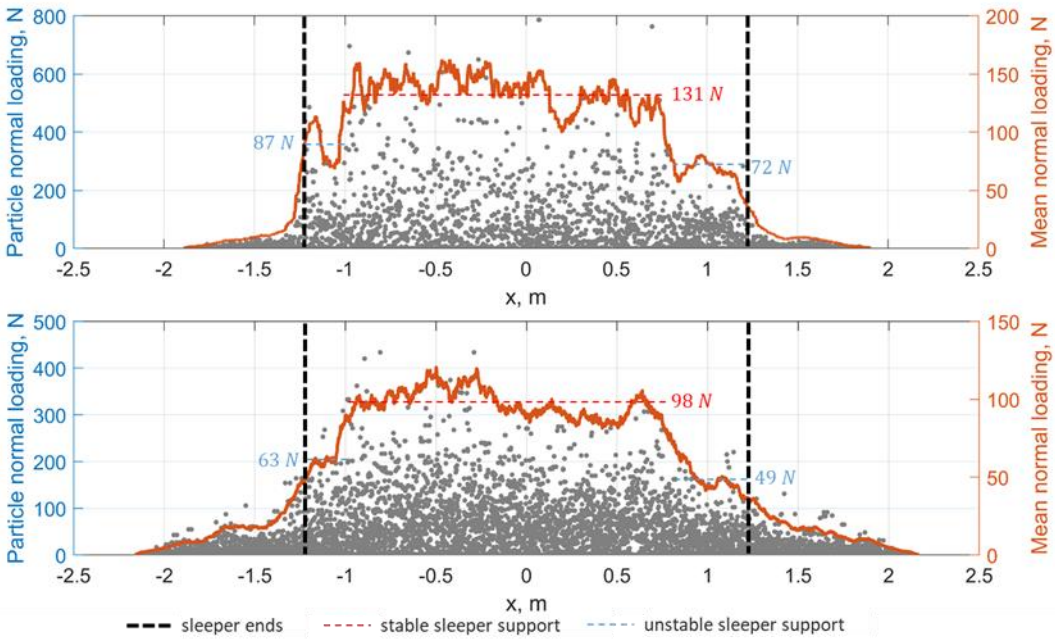


**Figure 22** The mean normal loading distribution in the particles under the sleeper (top) and over the subgrade (bottom) after the impact loading cycles

Preprints (www.preprints.org) | NOT PEER-REVIEWED | Posted: 2 July 2021 doi:10.20944/preprints202107.0066.v1

The parameters of the loading transmission can be interpreted as the angle of pressure distribution as was done in the other studies [49, 52, 54]. The angle of pressure distribution for the cyclic loading can be estimated as about 22°, and for the impact case - about 9°.

## 8. Discussion

The phenomenon of the intensive development of the unsupported sleeper zones is known for a long time. However, as the reasons of the development is usually considered the resulting geometrical irregularity and wheel-track dynamic interaction. The most of the present theoretical studies, despite the complex models used, simply imitate the experimental measurements and do not consider the internal reasons of the dynamic interaction. The experimental studies usually do not analyze the dynamic impact in the ballast-sleeper contact.

The present experimental measurements and the simple numerical modelling of the dynamic interaction indicates the presence of the ballast impact even for low velocity lightweight vehicles. Both results show that the impact occur not directly under the wheel but before it with some time shift. Moreover, some minor dynamic interaction occur during wheel leaving the void zone. Thereby, the wheel dynamic interaction is more than two times lower than that of the sleeper. Thus the main reason of is the impact is the void closing.

The simulated loading patterns of the ballast present quite different processes for the different locations of the void zone. The loading in the impact location consists of the short impact, the following quasistatical part and the full unloading before the impact. On the other hand, the neighbour to the void zones are characterized by a high pre-stress of the ballast and up to 2 times higher loading amplitudes than for the track without void. The other zones in the void have low impact and are lower quasistatically loaded depending on the void sizes.

The study of void sizes influence on the dynamic interaction shows ambiguous relations. Different to a geometrical irregularity, the influence of the void depth on the dynamic interaction, until some depth the loadings increase and after it should decrease until full unloading. Thus, the maximal impact values are present for some void depth.

The numerical simulation provides only an approximate imitation of the experimental measurement. It cannot itself explain the mechanism or the complex interrelations between the influencing factors and the impact loading. A simple analytical explanation is proposed by using the clamped beam as the basic model. The found equation for the sleeper impact velocity shows that it depends linearly to the train speed. It can explain why the low velocities cause high impacts. Thus, the dominating reason of the impact is not the wheel-track interaction but the rail qusistatic deflection rate. However, for high velocities, the resulting dynamic interaction could be a combination of both effects.

The DEM simulation of a sleeper settlements under the main ballast loading patterns in the void zone shows almost no increase of the settlement intensity for the pre-stressed ballast despite the 30% increase of the maximal loadings. However, the impact loading case caused more than 8 times higher settlement intensity. The influence of the pre-stress and impact factors is the aim of the further studies.

Thus the phenomenon of settlement intensity increase for the case of impact loading has a relation to property of the pressure distribution of the ballast layer and first of all the pressure breakdown zones under the sleeper ends. The growing zones can be explained with the reduction of the horizontal particle support of the ballast bed sides due to particle flow. The investigation of the further reason chain up to the root causes is the aim of the further research.

 doi:10.20944/preprints202107.0066.v1

## 9. Conclusions

The following main results can be concluded from the study:

1. The ballast impact appear due to void closing before the wheel.
2. Impact accelerations of the sleeper in a void zone are higher than corresponding wheel accelerations.
3. The ballast loading in the void zone is characterized with different loading patterns of impact and quasistatic loading that depend on the ballast support position along the void zone.
4. The maximal impact appear in some void depth.
5. The vertical impact velocity of sleepers depend linear of the longitudinal wheel velocity.
6. The impact loading in the void zone cause up to eight-time higher settlement intensity than for the normal weight loading without void.

**Author Contributions:** Conceptualization, M. Sysyn; writing-original draft preparation, M. Sysyn; review and editing, M. Przybylowicz; mechanical model development and case modelling, M. Przybylowicz, O. Nabochenko; experimental measurements processing, M. Sysyn; DEM simulation, M. Sysyn, J. Liu.

**Acknowledgments:** The authors acknowledge the support of Swiss Federal Railways with the experimental measurements.

**Conflicts of Interest:** The authors declare no conflict of interest.

## References

1. Grassie, S. L.; Cox, S. J. The dynamic response of railway track with unsupported sleepers, Proceedings of Institution of Mechanical Engineers (Part D), 199 (2). 1985, 123-135
2. Holtzendorff, K. Investigation of the settlement behaviour of railway ballast and the void forming on railway tracks; PhD Thesis, Technische Universität Berlin, 2003. (in German)
3. Lundqvist, A; Dahlberg, T. Load impact on railway track due to unsupported sleepers. Proc Inst Mech Eng, Part F: J Rail Rapid Transit 2005, 219, 2, 67–77. https://doi.org/10.1243/095440905X8790
4. Bezin, Y.; Iwnicki, S.D.; Cavalletti, M.; Vries, E.; Shahzad, F.; Evans, G. An investigation of sleeper voids using a flexible track model integrated with railway multi-bodydynamics. Proc Inst Mech Eng, Part F: J Rail Rapid Transit 2009, 223, 6, 597-607. https://doi.org/10.1243/09544097JRRT276
5. Zhu, J; Ahmed, AKW.; Rakheja, S; Khajepour, A. Development of a vehicle–track model assembly and numerical method for simulation of wheel–rail dynamic interaction due to unsupported sleepers. Veh Sys Dyn 2010, 48, 12, 1535-1552. https://doi.org/10.1080/00423110903540751
6. Kim, D.-S.; Kim, S. D.; Lee, J. Easy detection and dynamic behavior unsupported sleepers in high speed ballasted track, Proceeding of World Congress on Railway Research, Montreal, Canada (2006).
7. Zhang, S., Xiao, X., Wen, Z., Jin, X. Effect of unsupported sleepers on wheel/rail normal load, (2008) Soil Dynamics and Earthquake Engineering, 2007, 28 (8), pp. 662-673. doi: 10.1016/j.soildyn.2007.08.006
8. Recuero, A.M., Escalona, J.L., Shabana, A.A. Finite-element analysis of unsupported sleepers using three-dimensional wheel-rail contact formulation. Proceedings of the Institution of Mechanical Engineers, Part K: Journal of Multi-body Dynamics, 2011, 225(2), pp. 153-165. https://doi.org/10.1177/2041306810394971
9. Varandas, J.N., Hölscher, P., Silva, M.A.G. Dynamic behaviour of railway tracks on transitions zones. Computers and Structures, 2011, 89(13-14), pp. 1468-1479. https://doi.org/10.1016/j.compstruc.2011.02.013
10. Paixão, A., Fortunato, E., Calçada, R. The effect of differential settlements on the dynamic response of the train-track system: A numerical study, Engineering Structures,2015, 88, pp. 216-224. https://doi.org/10.1016/j.engstruct.2015.01.044
11. Zuada Coelho, B., Hicks, M.A. Numerical analysis of railway transition zones in soft soil, Proceedings of the Institution of Mechanical Engineers, Part F: Journal of Rail and Rapid Transit, 2016, 230(6), pp. 1601-1613. https://doi.org/10.1177/0954409715605864
12. Yoon, H.-J., Song, K.-Y., Choi, C., Na, H.-S., Kim, J.-S. Real-Time Distributed Strain Monitoring of a Railway Bridge during Train Passage by Using a Distributed Optical Fiber Sensor Based on Brillouin Optical Correlation Domain Analysis, Journal of Sensors, 2016,9137531. https://doi.org/10.1155/2016/9137531
13. Elsayed, H., Lotfy, M., Zohny, H., Sobhy, H. Assessment of degradation of railroad rails: Finite element analysis of insulated joints and unsupported sleepers, Journal of Mechanics of Materials and Structures, 2016, 14(3), pp. 429-448. https://doi.org/10.2140/jomms.2019.14.429

14. Auersch, L. Tracks with under-ballast plates and their mitigation of train induced ground vibration, 24th International Congress on Sound and Vibration, ICSV 2017
15. Zhang, D., Wang, K., Zhai, W., Liu, P. Effect of unsupported sleepers on the wheel/rail dynamic interaction on heavy-haul railway lines, Zhendong yu Chongji/Journal of Vibration and Shock, 2017, 36(18), pp. 1-7. https://doi.org/10.13465/j.cnki.jvs.2017.18.001
16. Tanigawa, H., Nakamura, T., Momoya, Y. Study on the evaluation of track support stiffness of the ballasted track using the fwd, Bearing Capacity of Roads, Railways and Airfields - Proceedings of the 10th International Conference on the Bearing Capacity of Roads, Railways and Airfields, BCRRA 2017, pp. 1945-1953. https://doi.org/10.1201/9781315100333-276
17. Kaynia, A.M., Park, J., Norén-Cosgriff, K. Effect of track defects on vibration from high speed train, Procedia Engineering, 2017, 199, pp. 2681-2686. https://doi.org/10.1016/j.proeng.2017.09.551
18. Mosayebi, S.-A., Esmaeili, M., Zakeri, J.-A. Numerical investigation of the effects of unsupported railway sleepers on train-induced environmental vibrations, Journal of Low Frequency Noise Vibration and Active Control, 2017, 36(2), pp. 160-176. https://doi.org/10.1177/0263092317711990
19. Li, H., Zhao, G., Cai, L. Effects of unsupported sleepers on dynamic response of ballast track structures on bridge, Beijing Jiaotong Daxue Xuebao/Journal of Beijing Jiaotong University, 2018, 42(4), pp. 19-26. https://doi.org/10.11860/j.issn.1673-0291.2018.04.003
20. Sun, Y., Guo, Y., Chen, Z., Zhai, W. Effect of Differential Ballast Settlement on Dynamic Response of Vehicle-Track Coupled Systems, International Journal of Structural Stability and Dynamics, 2018, 18(7),1850091. https://doi.org/10.1142/S0219455418500918
21. Germonpré, M., Degrande, G., Lombaert, G. Periodic track model for the prediction of railway induced vibration due to parametric excitation, Transportation Geotechnics, 2018, 17, pp. 98-108. https://doi.org/10.1016/j.trgeo.2018.09.015
22. Zhu, J. Y.; Thompson, D. J.; Jones, C. J. C. On the effect of unsupported sleepers on the dynamic behaviour of a railway track, Vehicle System Dynamics, 49 (9) (2011) 1389-1408.
23. Rezaei, E; Dahlberg, T. Dynamic behaviour of an in situ partially supported concrete railway sleeper. Proc Inst Mech Eng, Part F: J Rail Rapid Transit 2011, 225(5):501-508. https://doi.org/10.1177/2041301710392492
24. Sadeghi, J.; Zakeri, J.-A.; Reza, K. Effect of unsupported sleepers on rail track dynamic behaviour. Proceedings of the Institution of Civil Engineers: Transport 2018, 171, 5, 286-298. https://doi.org/10.1680/jtran.16.00161
25. Mosayebi, S.-A.; Zakeri, J.A.; Esmaeili, M; Effects of train bogie patterns on the mechanical performance of ballasted railway tracks with unsupported sleepers. Proceedings of the Institution of Mechanical Engineers, Part F: Journal of Rail and Rapid Transit 2018, 232, 1, 238-248. https://doi.org/10.1177/0954409716664932
26. Hamarat, M.; Papaelias, M.; Silvast, M.; Kaewunruen, S. The effect of unsupported sleepers/bearers on dynamic phenomena of a railway turnout system under impact loads. Applied Sciences (Switzerland) 2020, 10, 7, 2320. https://doi.org/10.3390/app10072320
27. Xu, L.; Zhao, Y.; Li, Z.; Shi, C.; Yu, Z.. Three-dimensional vehicle-ballasted track-subgrade interaction: Model construction and numerical analysis, Applied Mathematical Modelling 2020, 86, 424-445. https://doi.org/10.1016/j.apm.2020.05.007
28. Dai, J.; Ang, K.K.; Jiang, D. Moving element analysis of high-speed rail system accounting for hanging sleepers. MATEC Web of Conferences, 148, 05007. https://doi.org/10.1051/matecconf/201814805007
29. Blanco, B.; Alonso, A.; Kari, L.; Gil-Negrete, N.; Giménez, J.G. Distributed support modelling for vertical track dynamic analysis. Vehicle System Dynamics 2018, 56, 4, 529–552. https://doi.org/10.1080/00423114.2017.1394473
30. Lazarević, L; Vučković, D; Popović, Z. Assessment of sleeper support conditions using micro-tremor analysis. Proc Inst Mech Eng, Part F: J Rail and Rapid Transit 2015, 227, 6 ,657–667. https://doi.org/10.1177/0954409715615629
31. Balouchi, F; Bevan, A; Formston, R. Detecting railway under-track voids using multi-train in-service vehicle accelerometer. 7th IET Conference on Railway Condition Monitoring 2016 (RCM 2016), Birmingham, 2016, 1-6, https://doi.org10.1049/cp.2016.1194.
32. Pannese, E.M.; Take, W.A.; Hoult, N.A.; Yan, R.; Le, H. Bridge transition monitoring: Interpretation of track defects using digital image correlation and distributed fiber optic strain sensing. Proceedings of the Institution of Mechanical Engineers, Part F: Journal of Rail and Rapid Transit 2020, 234, 6, 616-637. https://doi.org/10.1177/0954409719851626
33. Wang, H., Markine, V., Liu, X. Experimental analysis of railway track settlement in transition zones. Proceedings of the Institution of Mechanical Engineers, Part F: Journal of Rail and Rapid Transit, 2018, 232, 6, 1774-1789. https://doi.org/10.1177/0954409717748789
34. Sabato, A.; Niezrecki, C. Feasibility of digital image correlation for railroad tie inspection and ballast support assessment. Measurement: Journal of the International Measurement Confederation 2017, 103, 93-105. https://doi.org/10.1016/j.measurement.2017.02.024
35. Phap, N.V., Bolshakova, A.V., Boronachin, A.M., Podgornaya, L.N., Shalymov, R.V. Vibration Analysis of a Railcar/Rail System using Inertial Sensors Mounted on Axle Boxes, Proceedings of the 2021 IEEE Conference of Russian Young Researchers in Electrical and Electronic Engineering, ElConRus 2021, 2021, 9396332, pp. 1659-1662. https://doi.org/10.1109/ElConRus51938.2021.9396332
36. Azizi, M., Shahravi, M., Zakeri, J.-A. Effect of unsupported sleepers on dynamic behavior of running vehicles and ride comfort index. Proceedings of the Institution of Mechanical Engineers, Part C: Journal of Mechanical Engineering Science, 2021, Article in Press. https://doi.org/10.1177/0954406221989371

37. Watanabe, T., Goto, K., Matsuoka, K., Minoura, S. Validation of a dynamic wheel load factor and the influence of various track irregularities on the dynamic response of prestressed concrete sleepers. Proceedings of the Institution of Mechanical Engineers, Part F: Journal of Rail and Rapid Transit, 2020,234(10), pp. 1275-1284. https://doi.org/10.1177/0954409719891655
38. Cui, X., Xiao, H., Xiao, H., Ma, C. DEM analysis of effect of unsupported sleepers on dynamic characteristics of ballast beds. Zhendong yu Chongji/Journal of Vibration and Shock, 2020, 39(16), pp. 171-179. https://doi.org/10.13465/j.cnki.jvs.2020.16.024
39. Wheeler, L.N., Andy Take, W., Hoult, N.A., Le, H. Use of fiber optic sensing to measure distributed rail strains and determine rail seat forces under a moving train, Canadian Geotechnical Journal, 2019, 56(1), pp. 1-13. https://doi.org/10.1139/cgj-2017-0163
40. Wu, Q., Sun, Y., Spiryagin, M., Cole, C. Parallel Co-Simulation Method for Railway Vehicle-Track Dynamics, Journal of Computational and Nonlinear Dynamics, 2018, 13(4),041004
41. Sun, Y.Q., Spiryagin, M., Cole, C. Simulations of wheel-rail dynamics due to track ballast voids. The Dynamics of Vehicles on Roads and Tracks, 2018, 2, pp. 687-692. https://doi.org/10.1115/1.4039310
42. Joh, S.-H., Magno, K., Hwang, S.H. Dynamic deflection of a railroad sleeper from the coupled measurements of acceleration and strain, Sensors (Switzerland), 2018, 18(7),2182. https://doi.org/10.3390/s18072182
43. Sysyn, M., Nabochenko, O., Kovalchuk, V. Experimental investigation of the dynamic behavior of railway track with sleeper voids, Railway Engineering Science, 2020, 28 (3), pp. 290-304, https://doi.org/10.1007/s40534-020-00217-8
44. Sysyn, M., Przybylowicz, M., Nabochenko, O., Kou, L. Identification of sleeper support conditions using mechanical model supported data-driven approach, Sensors, 2021, 21(11), 3609, https://doi.org/10.3390/s21113609
45. Xu, J., Butler, L.J., Elshafie, M.Z.E.B. Experimental and numerical investigation of the performance of self-sensing concrete sleepers, Structural Health Monitoring, 2020,19(1), pp. 66-85. https://doi.org/10.1177/1475921719834506
46. Jing, G., Siahkouhi, M., Riley Edwards, J., Dersch, M.S., Hoult, N.A. Smart railway sleepers - a review of recent developments, challenges, and future prospects, Construction and Building Materials, 271,121533. https://doi.org/10.1016/j.conbuildmat.2020.121533
47. Pletscher, S. Erhebung und Auswertung von Messdaten des Schwingweges von Einzelfehlern im Gleis. Master Thesis. ETH Zürich, 2020. (in German)
48. Wensrich, C.M., Katterfeld, A. Rolling friction as a technique for modelling particle shape in DEM. Powder Technology, 2012, 217, pp. 409-417. https://doi.org/10.1016/j.powtec.2011.10.057
49. Lichtberger, B. Track compendium: formation, permanent way, maintenance, economics; Eurailpress: Hamburg,Germany, 2005.
50. Highway Research Board: Special Report 61-G: The AASHO Road Test, Report 7 / Highway Research Board Washington, D.C. 1962. – Forschungsbericht
51. Sysyn, M., Gerber, U., Kovalchuk, V., Nabochenko, O. The complex phenomenological model for prediction of inhomogeneous deformations of railway ballast layer after tamping works. Archives of Transport, 2018, 46(3), pp. 91–107. https://doi.org/10.5604/01.3001.0012.6512
52. Sysyn, M., Gerber, U., Nabochenko, O., Dehne, S., 2020, A Laboratory Study of Pressure Distribution and Residual Settlements in Wide Grading Double Layer Railway Ballast under Long-Term Cyclic Loading, Archives of Civil Engineering, 64(2), pp. 561-578
53. Baessler M., Ruecker W (2003) Track Settlement Due to Cyclic Loading with Low Minimum Pressure and Vibrations. In Popp K., Schiehlen W. (eds) System Dynamics and Long-Term Behaviour of Railway Vehicles, Track and Subgrade. Lecture Notes in Applied Mechanics, vol 6. Springer, Berlin, Heidelberg
54. Sysyn, M., Kovalchuk, V., Nabochenko, O., Kovalchuk, Y., Voznyak, O. Experimental study of railway trackbed pressure distribution under dynamic loading. Baltic Journal of Road and Bridge Engineering, 2019, 14(4), pp. 504–520. https://doi.org/10.7250/bjrbe.2019-14.455
55. A. Böge, W. Böge.Handbuch Maschinenbau: Grundlagen und Anwendungen der Maschinenbau-Technik. Springer Fachmedien Wiesbaden 2014, 1524 p. https://doi.org/10.1007/978-3-658-06598-0 (in German)
56. Г.С. Писаренко, А.П. Яковлев, В.В. Матвеев. Справочник по сопротивлению материалов. Наукова думка. Киев. 1988, 736p. (in Russian)
57. Lim, W. L., and G. R. McDowell. Discrete element modelling of railway ballast. Granular Matter, 2005, 7(1), pp. 19-29.
58. Tutumluer E, Qian Y, Hashash Y M A, et al. Discrete element modelling of ballasted track deformation behaviour[J]. International Journal of Rail Transportation, 2013, 1(1-2), pp. 57-73.
59. Indraratna B, Ngo N T, Rujikiatkamjorn C, et al. Behavior of fresh and fouled railway ballast subjected to direct shear testing: discrete element simulation. International Journal of Geomechanics, 2014, 14(1), pp. 34-44.
60. Juhász, E., Fischer, S. Tutorial on the fragmentation of the railway ballast particles and calibration methods in discrete element modelling. Acta Technica Jaurinensis, 2021, 14(1), 104–122. https://doi.org/10.14513/actatechjaur.00569
61. Juhasz, E., Movahedi, R. M., Fekete, I., & Fischer, S. DISCRETE ELEMENT MODELLING OF PARTICLE DEGARDATION OF RAILWAY BALLAST MATERIAL WITH PFC3D SOFTWARE. Science and Transport Progress. Bulletin of Dnipropetrovsk National University of Railway Transport, 2019, 6(84), 103–116. https://doi.org/10.15802/stp2019/194472
62. Orosz, A., Zwierczyk, P.T. Analysis of the stress state of a railway sleeper using coupled fem-dem simulation. Proceedings - European Council for Modelling and Simulation, ECMS, 2020, 34(1), pp. 261–265
63. Jing G, Luo Q, Wang Z, et al. Micro-analysis of hanging sleeper dynamic interactions with ballast bed. Journal of Vibroengineering, 2015, 17(1), pp. 444-454.

 doi:10.20944/preprints202107.0066.v1

64. Liu, Jianxing, et al. Settlement and Stress Distribution Characteristics of a Railway Ballast Layer under a Dynamic Load. No. TRBAM-21-00414. 2021.
65. Guo Y, Zhao C, Markine V, et al. Discrete element modelling of railway ballast performance considering particle shape and rolling resistance. Railway Engineering Science, 2020, 28(4), pp. 382-407.